Probabilistic Engineering Mechanics 77 (2024) 103666

Contents lists available at ScienceDirect

Probabilistic Engineering Mechanics

journal homepage: www.elsevier.com/locate/probengmech

Higher-order moments of spline chaos expansion ☆

Sharif Rahman [1]

College of Engineering, The University of Iowa, Iowa City, IA 52242, USA

ARTICLE INFO

Keywords:
Uncertainty quantification
B-splines
Orthonormal splines
Variance
Skewness
Kurtosis
Polynomial chaos expansion
Modulus of smoothness
Error analysis

ABSTRACT

Spline chaos expansion, referred to as SCE, is a finite series representation of an output random variable in terms of measure-consistent orthonormal splines in input random variables and deterministic coefficients. This paper reports new results from an assessment of SCE's approximation quality in calculating higher-order moments, if they exist, of the output random variable. A novel mathematical proof is provided to demonstrate that the moment of SCE of an arbitrary order converges to the exact moment for any degree of splines as the largest element size decreases. Complementary numerical analyses have been conducted, producing results consistent with theoretical findings. A collection of simple yet relevant examples is presented to grade the approximation quality of SCE with that of the well-known polynomial chaos expansion (PCE). The results from these examples indicate that higher-order moments calculated using SCE converge for all cases considered in this study. In contrast, the moments of PCE of an order larger than two may or may not converge, depending on the regularity of the output function or the probability measure of input random variables. Moreover, when both SCE- and PCE-generated moments converge, the convergence rate of the former is markedly faster than the latter in the presence of nonsmooth functions or unbounded domains of input random variables.

1. Introduction

Uncertainty quantification (UQ) is the science of quantitative characterization and management of uncertainties in computational modeling, simulation, and design of complex engineering systems [1,2]. There exists a myriad of UQ methods or expansions, namely, polynomial chaos expansion (PCE) [3–5], polynomial dimensional decomposition, [6,7], stochastic collocation [8,9], and sparse-grid quadrature [10, 11], to name just four. These methods and a few others not explicitly cited for brevity offer significant computational advantages over crude Monte Carlo simulation (MCS), especially when the output variable is globally smooth over the entire domain of input random variables. More recently, the author's group has delved into spline chaos expansion (SCE) [12], followed by spline dimensional decomposition (SDD) [13], for deftly handling UQ problems featuring locally prominent responses, including discontinuous or nonsmooth solutions. The latter two methods prominently feature orthogonalized basis splines (B-splines), albeit standard B-splines have been used as well [14].

Once an expansion of an output random variable of interest has been generated, the natural progression is to develop explicit formulae, if they exist, for calculating its second-moment properties. If the expansion is founded on measure-consistent orthogonal bases, such as those rooted in PCE and SCE, then closed-form expressions of the mean and variance of the output variable can be obtained easily. While these second-moment properties are important, additional statistical measures, such as skewness and kurtosis, are also valuable and may be necessary in evaluating complex system performance. Therefore, in general, the approximation quality and convergence properties of these expansions in calculating not only the first- and second-order moments but also higher-order moments should be examined thoroughly. Such a need stems from the fact that the accuracy of an estimated probabilistic characteristic of the output variable, often required in reliability analysis and design, strongly depends on whether or not the higher-order moment approximations converge or diverge with respect to the expansion order or truncation parameters of a UQ method.

The focus of this study is the approximation quality of SCE in calculating high-order moments of a random variable of interest. A novel mathematical proof and complementary numerical analysis have been reported. Therefore, compared with the past works on SCE, which entail mostly second-moment analysis, the results of this paper are new. The paper is organized as follows. Section 2 begins with mathematical preliminaries and requisite assumptions on input and output random variables. Section 3 summarizes the construction of measure-consistent orthonormalized B-splines, leading to the SCE approximation, and output moments. Section 4 describes new theoretical results of error analysis, proving convergence of SCE-generated moments for

☆ Grant sponsors: U.S. Department of Education (Grant No. P116S210005); U.S. National Science Foundation (Grant No. CMMI-2317172).
E-mail address: sharif-rahman@uiowa.edu.
[1] Professor.

https://doi.org/10.1016/j.probengmech.2024.103666
Received 27 April 2024; Received in revised form 28 June 2024; Accepted 15 July 2024
Available online 22 July 2024

an arbitrary order. Four illustrative numerical examples comprising elementary mathematical functions of single or multiple input random variable(s) with bounded or unbounded random domains are presented in Section 5. Section 6 discusses limitations of the current study and future work. Finally, conclusions are drawn in Section 7.

2. Random variables

Let $\mathbb{N} := \{1, 2, \ldots\}$, $\mathbb{N}_0 := \mathbb{N} \cup \{0\}$, and $\mathbb{R} := (-\infty, +\infty)$ represent the sets of positive integer (natural), non-negative integer, and real numbers, respectively. Denote by $[a_k, b_k]$ a finite closed interval, where $a_k, b_k \in \mathbb{R}$, $b_k > a_k$. Then, given $N \in \mathbb{N}$, $\mathbb{A}^N = \times_{k=1}^N [a_k, b_k]$ represents a closed bounded domain of $\mathbb{R}^N$.

2.1. Input

Let $(\Omega, \mathcal{F}, \mathbb{P})$ be a probability space, where Ω is a sample space representing an abstract set of elementary events, $\mathcal{F}$ is a σ-algebra on Ω, and $\mathbb{P} : \mathcal{F} \to [0, 1]$ is a probability measure. Defined on this probability space, consider an N-dimensional input random vector $\mathbf{X} := (X_1, \ldots, X_N)^\intercal$, describing the statistical uncertainties in all system parameters of a stochastic or UQ problem. Denote by $F_{\mathbf{X}}(\mathbf{x}) := \mathbb{P}(\cap_{i=1}^N \{X_k \le x_k\})$ the joint distribution function of $\mathbf{X}$. The kth component of $\mathbf{X}$ is a random variable X_k, which has the marginal probability distribution function $F_{X_k}(x_k) := \mathbb{P}(X_k \le x_k)$. In the UQ community, the input random variables are also known as basic random variables. The non-zero, finite integer N represents the number of input random variables and is often referred to as the dimension of the stochastic or UQ problem.

A set of assumptions on input random variables used or required by SCE is as follows.

Assumption 1. The input random vector $\mathbf{X} := (X_1, \ldots, X_N)^\intercal$ satisfies all of the following conditions:

(1) All component random variables X_k, $k = 1, \ldots, N$, are statistically independent, but not necessarily identical.

(2) Each input random variable X_k is defined on a bounded interval $[a_k, b_k] \subset \mathbb{R}$. Therefore, all moments of X_k exist, that is, for all $l \in \mathbb{N}_0$,

$$\mathbb{E}\left[X_k^l\right] := \int_\Omega X_k^l(\omega) d\mathbb{P}(\omega) < \infty, \tag{1}$$

where $\mathbb{E}$ is the expectation operator with respect to the probability measure $\mathbb{P}$.

(3) Each input random variable X_k has absolutely continuous marginal probability distribution function $F_{X_k}(x_k)$ and continuous marginal probability density function $f_{X_k}(x_k) := \partial F_{X_k}(x_k)/\partial x_k$ with a bounded support $[a_k, b_k] \subset \mathbb{R}$. Consequently, with Items (1) and (2) in mind, the joint probability distribution function $F_{\mathbf{X}}(\mathbf{x})$ and joint probability density function (PDF) $f_{\mathbf{X}}(\mathbf{x}) := \partial^N F_{\mathbf{X}}(\mathbf{x})/\partial x_1 \cdots \partial x_N$ of $\mathbf{X}$ are obtained from

$$F_{\mathbf{X}}(\mathbf{x}) = \prod_{k=1}^N F_{X_k}(x_k) \quad \text{and} \quad f_{\mathbf{X}}(\mathbf{x}) = \prod_{k=1}^N f_{X_k}(x_k),$$

respectively, with a bounded support $\mathbb{A}^N \subset \mathbb{R}^N$ of the density function.

Assumption 1 establishes the existence of a relevant sequence of orthogonal polynomials or splines consistent with the input probability measure. The discrete distributions and dependent variables are not dealt with in this paper.

Given the abstract probability space $(\Omega, \mathcal{F}, \mathbb{P})$ of $\mathbf{X}$, there exists an image probability space $(\mathbb{A}^N, \mathcal{B}^N, f_{\mathbf{X}} d\mathbf{x})$, where $\mathbb{A}^N$ is the image of Ω from the mapping $\mathbf{X} : \Omega \to \mathbb{A}^N$ and $\mathcal{B}^N := \mathcal{B}(\mathbb{A}^N)$ is the Borel σ-algebra on $\mathbb{A}^N \subset \mathbb{R}^N$. Relevant statements and objects in the abstract probability space have obvious counterparts in the associated image probability space. Both probability spaces will be exploited in this paper.

2.2. Output

Given an input random vector $\mathbf{X} := (X_1, \ldots, X_N)^\intercal : (\Omega, \mathcal{F}) \to (\mathbb{A}^N, \mathcal{B}^N)$ with known PDF $f_{\mathbf{X}}(\mathbf{x})$ on $\mathbb{A}^N \subset \mathbb{R}^N$, denote by $y(\mathbf{X}) := y(X_1, \ldots, X_N)$ a real-valued, measurable transformation on $(\Omega, \mathcal{F})$, describing a general output response of a stochastic system. A major objective of UQ analysis is to estimate the statistical and probabilistic characteristics of an output random variable $Y = y(\mathbf{X})$, including its statistical moments and PDF, when the probability law of the input random vector $\mathbf{X}$ is prescribed. More often than not, Y is assumed to belong to a class of random variables, such as the weighted L^p space

$$L^p(\Omega, \mathcal{F}, \mathbb{P}) := \Bigg\{ Y : \Omega \to \mathbb{R} : \int_\Omega |y(\mathbf{X}(\omega))|^p \, d\mathbb{P}(\omega) = \int_{\mathbb{A}^N} |y(\mathbf{x})|^p f_{\mathbf{X}}(\mathbf{x}) \, d\mathbf{x} < \infty \Bigg\}, \tag{2}$$

where $2 \le p < \infty$ is an integer and $y(\mathbf{x})$ is a member of the associated $L^p(\mathbb{A}^N, \mathcal{B}^N, f_{\mathbf{X}} d\mathbf{x})$ space of real-valued p-integrable functions. In other words, L^p is a class of all random variables on the probability space $(\Omega, \mathcal{F}, \mathbb{P})$ that have at most finite p-order moments. This is a normed linear space with the L^p norm, defined by

$$\|y(\mathbf{X})\|_{L^p(\Omega,\mathcal{F},\mathbb{P})} := \left(\int_\Omega |y(\mathbf{X}(\omega))|^p \, d\mathbb{P}(\omega) \right)^{1/p} = \left(\int_{\mathbb{A}^N} |y(\mathbf{x})|^p f_{\mathbf{X}}(\mathbf{x}) \, d\mathbf{x} \right)^{1/p}. \tag{3}$$

When $p = 2$, the resultant L^2 space becomes a Hilbert space endowed with the inner product

$$(y(\mathbf{X}), z(\mathbf{X}))_{L^2(\Omega,\mathcal{F},\mathbb{P})} := \int_\Omega y(\mathbf{X}(\omega)) z(\mathbf{X}(\omega)) \, d\mathbb{P}(\omega) = \int_{\mathbb{A}^N} y(\mathbf{x}) z(\mathbf{x}) f_{\mathbf{X}}(\mathbf{x}) \, d\mathbf{x} \tag{4}$$

and the associated norm

$$\|y(\mathbf{X})\|_{L^2(\Omega,\mathcal{F},\mathbb{P})} := \sqrt{(y(\mathbf{X}), y(\mathbf{X}))_{L^2(\Omega,\mathcal{F},\mathbb{P})}} = \sqrt{\int_\Omega y^2(\mathbf{X}(\omega)) \, d\mathbb{P}(\omega)} = \sqrt{\int_{\mathbb{A}^N} y^2(\mathbf{x}) f_{\mathbf{X}}(\mathbf{x}) \, d\mathbf{x}}. \tag{5}$$

It is elementary to show that $y(\mathbf{X}(\omega)) \in L^p(\Omega, \mathcal{F}, \mathbb{P})$ if and only if $y(\mathbf{x}) \in L^p(\mathbb{A}^N, \mathcal{B}^N, f_{\mathbf{X}} d\mathbf{x})$. Therefore, convergence of random variables Y and functions $y(\mathbf{x})$ from these two related L^p spaces can be studied interchangeably.

3. Spline chaos expansion

In this section, the SCE method exploiting measure-consistent B-splines is described for solving a generic UQ problem subject to the assumptions listed in Section 2. The method is founded on Fourier-spline expansion of any p-integrable output function of interest.

3.1. Standard univariate B-splines

Let $\mathbf{x} = (x_1, \ldots, x_N)$ be an arbitrary point in $\mathbb{A}^N$. For the coordinate direction k, $k = 1, \ldots, N$, define a non-negative integer $m_k \in \mathbb{N}_0$ and a positive integer $n_k \ge m_k + 1$, representing the degree or order[2] and total number of basis functions, respectively. The rest of this section briefly describes necessary details of univariate B-splines.

For the coordinate direction $k = 1, \ldots, N$, define a knot vector

$$\boldsymbol{\xi}_k := \{\xi_{k,i_k}\}_{i_k=1}^{n_k+m_k+1} = \{a_k = \xi_{k,1}, \xi_{k,2}, \ldots, \xi_{k,n_k+m_k+1} = b_k\} \tag{6}$$

[2] Degree and order are used interchangeably in this paper.

on the interval $[a_k, b_k]$ by a non-decreasing sequence of real numbers, where ξ_{k,i_k} is the i_kth knot with $i_k = 1, 2, \ldots, n_k + m_k + 1$. Any knot may appear up to $m_k + 1$ times in the sequence. Hence, the knot vector can be rewritten as

$$\begin{aligned}\boldsymbol{\xi}_k = \{a_k = \overbrace{\zeta_{k,1}, \ldots, \zeta_{k,1}}^{M_{k,1}\text{ times}}, \overbrace{\zeta_{k,2}, \ldots, \zeta_{k,2}}^{M_{k,2}\text{ times}}, \ldots,\\ \overbrace{\zeta_{k,r_k-1}, \ldots, \zeta_{k,r_k-1}}^{M_{k,r_k-1}\text{ times}}, \overbrace{\zeta_{k,r_k}, \ldots, \zeta_{k,r_k}}^{M_{k,r_k}\text{ times}} = b_k\},\\ a_k = \zeta_{k,1} < \zeta_{k,2} < \cdots < \zeta_{k,r_k-1} < \zeta_{k,r_k} = b_k,\end{aligned} \tag{7}$$

where ζ_{k,j_k}, $j_k = 1, 2, \ldots, r_k$, are r_k unique knots, each of which has multiplicity $1 \le M_{k,j_k} \le m_k + 1$. For more details, readers are referred to Appendix A of this paper and Chapter 2 of the book by Cottrell et al. [15]. A knot vector is called $(m_k + 1)$-open if the end knots have multiplicities $m_k + 1$. In this work, only $(m_k + 1)$-open knot vectors are considered.

Denote by $B^k_{i_k,m_k,\boldsymbol{\xi}_k}(x_k)$ the i_kth univariate B-spline with degree m_k. Given the knot vector $\boldsymbol{\xi}_k$ and *zero*-degree basis functions, all higher-order B-spline functions on $[a_k, b_k]$ are defined recursively, where $1 \le k \le N$, $1 \le i_k \le n_k$, and $1 \le m_k < \infty$. See Appendix A for an explicit definition of $B^k_{i_k,m_k,\boldsymbol{\xi}_k}(x_k)$.

The B-splines encompass a number of mathematically desirable properties, endowing superb approximating power to numerical methods. More precisely, they are [15,16]: (1) non-negative; (2) locally supported on the interval $[\xi_{k,i_k}, \xi_{k,i_k+m_k+1})$ for all i_k; (3) linearly independent; (4) committed to partition of unity; and (5) pointwise C^∞-continuous everywhere except at the knots ζ_{k,j_k} of multiplicity M_{k,j_k} for all j_k, where they are $C^{p_k - M_{k,j_k}}$-continuous, provided that $1 \le M_{k,j_k} < m_k + 1$.

3.2. Orthonormalized univariate B-splines

The aforementioned B-splines, although they form a basis of the spline space of degree m_k and knot vector $\boldsymbol{\xi}_k$, are not necessarily orthogonal with respect to the probability measure $f_{X_k}(x_k)\,\mathrm{d}x_k$ of X_k. A three-step procedure, originally proposed in a past work [12], is summarized here to generate their orthonormal version.

(1) Given a set of B-splines of degree m_k, create an auxiliary set by replacing any element, arbitrarily chosen to be the first, with *one*. Arrange the elements of the set into an n_k-dimensional vector

$$\mathbf{P}_k(x_k) := \left(1, B^k_{2,m_k,\boldsymbol{\xi}_k}(x_k), \ldots, B^k_{n_k,m_k,\boldsymbol{\xi}_k}(x_k)\right)^\intercal \tag{8}$$

comprising the auxiliary B-splines. The linear independence of the auxiliary B-splines is preserved [12].

(2) Construct an $n_k \times n_k$ spline moment matrix

$$\mathbf{G}_k := \mathbb{E}[\mathbf{P}_k(X_k)\mathbf{P}_k^\intercal(X_k)]. \tag{9}$$

The matrix $\mathbf{G}_k$ exists because X_k has finite moments up to order $2m_k$, as stated in Assumption 1. Furthermore, it is symmetric and positive-definite [12], ensuring the existence of a non-singular $n_k \times n_k$ whitening matrix $\mathbf{W}_k$ such that

$$\mathbf{W}_k^\intercal \mathbf{W}_k = \mathbf{G}_k^{-1}. \tag{10}$$

(3) Apply a whitening transformation to create a vector of orthonormalized B-splines

$$\boldsymbol{\psi}_k(x_k) = \mathbf{W}_k \mathbf{P}_k(x_k), \tag{11}$$

consisting of uncorrelated components

$$\psi^k_{i_k,m_k,\boldsymbol{\xi}_k}(x_k), \quad i_k = 1, \ldots, n_k, \quad k = 1, \ldots, N.$$

Note that the invertibility of $\mathbf{G}_k$ does not uniquely determine $\mathbf{W}_k$. Indeed, there are several ways to choose $\mathbf{W}_k$ such that the condition described in Step (2) is satisfied [12]. One prominent, relatively stable option is to invoke the Cholesky factorization $\mathbf{G}_k = \mathbf{Q}_k \mathbf{Q}_k^\intercal$, leading to

$$\mathbf{W}_k = \mathbf{Q}_k^{-1}, \tag{12}$$

where $\mathbf{Q}_k$ is an $n_k \times n_k$ lower-triangular matrix. As a result, the transformation in Step (3) becomes

$$\boldsymbol{\psi}_k(x_k) = \mathbf{Q}_k^{-1} \mathbf{P}_k(x_k), \tag{13}$$

where the orthonormal splines are obtained by linear combinations of auxiliary B-splines. The rest of the paper will use the Cholesky factorization.

Fig. 1(a) presents a set of six second-order ($m = 2$) B-spline functions on $[-1, 1]$ with the uniformly spaced knot sequence $\boldsymbol{\xi} = \{-1, -1, -1, -0.5, 0, 0.5, 1, 1, 1\}$, obtained using the Cox-de Boor formula from Appendix A. They are non-negative and locally supported but not orthonormal with respect to the probability measure of the random variable X defined on $[-1, 1]$. When orthonormalized with respect to the uniform, truncated Gaussian, and Beta probability measures supported on $[-1, 1]$, as reported in a prior work [13], the respective basis functions are illustrated in Figs. 1(b), 1(c), and 1(d). The orthonormalized versions depend not only on the spacing of knots but also on the probability measure of X. Note that after orthonormalization, the non-constant B-splines are neither non-negative nor locally supported. However, since the orthormalized B-splines are linear combinations of standard B-splines, the former inherits all desirable properties of the latter.

3.3. Multivariate orthonormalized basis

The input random vector $\mathbf{X}$, as it comprises independent components, is endowed with a product-type probability measure. Therefore, multivariate orthonormalized B-splines in N variables are readily constructed from an N-dimensional tensor product of univariate orthonormalized B-splines, resulting in SCE.

Define three multi-indices $\mathbf{i} := (i_1, \ldots, i_N) \in \mathbb{N}^N$, $\mathbf{n} := (n_1, \ldots, n_N) \in \mathbb{N}^N$, and $\mathbf{m} := (m_1, \ldots, m_N) \in \mathbb{N}_0^N$, representing the knot indices, numbers of basis functions, and degrees of splines, respectively, in all N coordinate directions. Denote by $\boldsymbol{\Xi} := \{\boldsymbol{\xi}_1, \ldots, \boldsymbol{\xi}_N\}$ a family of all N knot vectors. Associated with $\mathbf{i}$, define an index set

$$\mathcal{I}_{\mathbf{n}} := \left\{\mathbf{i} = (i_1, \ldots, i_N) : 1 \le i_k \le n_k,\ k = 1, \ldots, N\right\} \subset \mathbb{N}^N \tag{14}$$

with cardinality

$$|\mathcal{I}_{\mathbf{n}}| = \prod_{k=1}^{N} n_k. \tag{15}$$

For the coordinate direction k, define by

$$I_k := r_k - 1 \tag{16}$$

the number of subintervals corresponding to the knot vector $\boldsymbol{\xi}_k$ with r_k distinct knots. Then the partition defined by the knot sequences $\boldsymbol{\xi}_k$, $k = 1, \ldots, N$, splits $\mathbb{A}^N := \times_{k=1}^N [a_k, b_k]$ into smaller N-dimensional rectangles

$$\left\{\mathbf{x} = (x_1, \ldots, x_N) : \zeta_{k,j_k} \le x_k < \zeta_{k,j_k+1},\ k = 1, \ldots, N\right\},\ j_k = 1, \ldots, I_k,$$

where ζ_{k,j_k} is the j_kth distinct knot in the coordinate direction k. A mesh is defined by a partition of $\mathbb{A}^N$ into such rectangular elements. Define the largest element size in each coordinate direction k by

$$h_k := \max_{j_k = 1, \ldots, I_k} \left(\zeta_{k,j_k+1} - \zeta_{k,j_k}\right),\ k = 1, \ldots, N. \tag{17}$$

Then, given the family of knot sequences $\boldsymbol{\Xi} = \{\boldsymbol{\xi}_1, \ldots, \boldsymbol{\xi}_N\}$,

$$\mathbf{h} := (h_1, \ldots, h_N) \quad \text{and} \quad h := \max_{k=1,\ldots,N} h_k \tag{18}$$

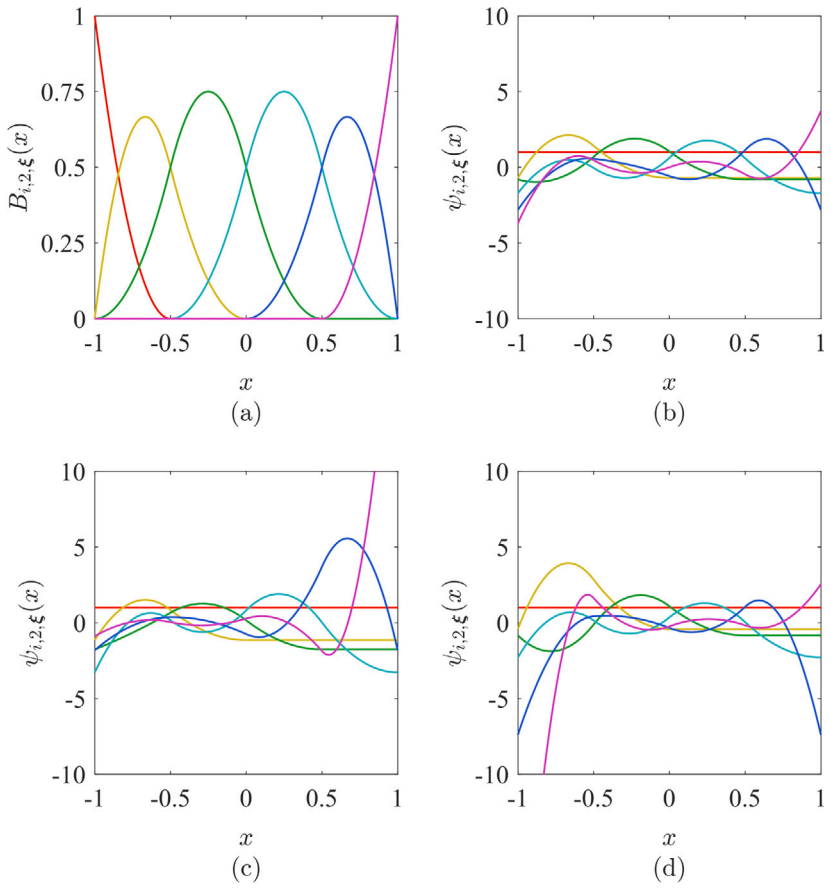

Fig. 1. A set of B-splines associated with the knot sequence $\xi = \{-1, -1, -1, -0.5, 0, 0.5, 1, 1, 1\}$ and degree $m = 2$ [13]; (a) non-orthonormal basis; (b) orthonormal basis for uniform measure; (c) orthonormal basis for truncated Gaussian measure; (d) orthonormal basis for Beta measure.

define a vector of the largest element sizes in all N coordinates and the global element size, respectively, for the domain $\mathbb{A}^N$. As a result, the multivariate orthonormalized B-splines in $\mathbf{x}$ consistent with the probability measure $f_{\mathbf{X}}(\mathbf{x})d\mathbf{x}$ are obtained from the product

$$\Psi_{\mathbf{i},\mathbf{m},\Xi}(\mathbf{x}) := \prod_{k=1}^{N} \psi^k_{i_k,m_k,\xi_k}(x_k), \quad \mathbf{i} = (i_1, \ldots, i_N) \in \mathcal{I}_{\mathbf{n}}. \tag{19}$$

Associated with $\mathbf{m} = \{m_1, \ldots, m_N\}$ and $\Xi = \{\xi_1, \ldots, \xi_N\}$, define a tensor-product spline space

$$S_{\mathbf{m},\Xi} := \bigotimes_{k=1}^{N} \text{span}\left\{\psi^k_{i_k,m_k,\xi_k}(x_k)\right\}_{i_k=1,\ldots,n_k}, \tag{20}$$

where the symbol $\bigotimes$ stands for tensor product. It is elementary to show that $\{\Psi_{\mathbf{i},\mathbf{m},\Xi}(\mathbf{x}) : \mathbf{i} \in \mathcal{I}_{\mathbf{n}}\}$ is a basis of $S_{\mathbf{m},\Xi}$.

When the input random variables $X_1, \ldots, X_N$, instead of real variables $x_1, \ldots, x_N$, are inserted in the argument, the multivariate splines $\Psi_{\mathbf{i},\mathbf{m},\Xi}(\mathbf{X})$, $\mathbf{i} \in \mathcal{I}_{\mathbf{n}}$, become functions of input random variables. Their second-moment properties are [12]

$$\mathbb{E}\left[\Psi_{\mathbf{i},\mathbf{m},\Xi}(\mathbf{X})\right] = \begin{cases} 1, & \mathbf{i} = \mathbf{1} := (1, \ldots, 1), \\ 0, & \mathbf{i} \neq \mathbf{1}, \end{cases} \tag{21}$$

and

$$\mathbb{E}\left[\Psi_{\mathbf{i},\mathbf{m},\Xi}(\mathbf{X})\Psi_{\mathbf{j},\mathbf{p},\Xi}(\mathbf{X})\right] = \begin{cases} 1, & \mathbf{i} = \mathbf{j}, \\ 0, & \mathbf{i} \neq \mathbf{j}. \end{cases} \tag{22}$$

3.4. SCE approximation

Given a degree $\mathbf{m}$ and a family of knot sequences Ξ, recall that $\{\Psi_{\mathbf{i},\mathbf{m},\Xi}(\mathbf{X}) : \mathbf{i} \in \mathcal{I}_{\mathbf{n}}\}$ represents the set comprising multivariate orthonormalized B-splines that is consistent with the probability measure $f_{\mathbf{X}}(\mathbf{x})d\mathbf{x}$. Then, for any random variable $y(\mathbf{X}) \in L^p(\Omega, \mathcal{F}, \mathbb{P})$, $2 \leq p < \infty$, there exists an orthogonal expansion in multivariate orthonormal splines in $\mathbf{X}$, referred to as an SCE approximation [12]

$$y_{\mathbf{m},\Xi}(\mathbf{X}) := \sum_{\mathbf{i} \in \mathcal{I}_{\mathbf{n}}} C_{\mathbf{i},\mathbf{m},\Xi}\Psi_{\mathbf{i},\mathbf{m},\Xi}(\mathbf{X}) \tag{23}$$

of $y(\mathbf{X})$, where the SCE expansion coefficients $C_{\mathbf{i},\mathbf{m},\Xi} \in \mathbb{R}$, $\mathbf{i} \in \mathcal{I}_{\mathbf{n}}$, are defined as

$$C_{\mathbf{i},\mathbf{m},\Xi} := \mathbb{E}\left[y(\mathbf{X})\Psi_{\mathbf{i},\mathbf{m},\Xi}(\mathbf{X})\right] := \int_{\mathbb{A}^N} y(\mathbf{x})\Psi_{\mathbf{i},\mathbf{m},\Xi}(\mathbf{x})f_{\mathbf{X}}(\mathbf{x})d\mathbf{x}, \quad \mathbf{i} \in \mathcal{I}_{\mathbf{n}}. \tag{24}$$

Strictly speaking, the SCE approximation in (23) was originally defined for $y(\mathbf{X}) \in L^2(\Omega, \mathcal{F}, \mathbb{P})$. Since the probability measure is a finite measure and $2 \leq p < \infty$, $L^p(\Omega, \mathcal{F}, \mathbb{P}) \subseteq L^2(\Omega, \mathcal{F}, \mathbb{P})$. Therefore, the SCE approximation is also applicable for $y(\mathbf{X}) \in L^p(\Omega, \mathcal{F}, \mathbb{P})$.

According to (23), the SCE of any random variable $y(\mathbf{X}) \in L^p(\Omega, \mathcal{F}, \mathbb{P})$ is an orthogonal projection onto the spline space $S_{\mathbf{m},\Xi}$ spanning the set of measure-consistent multivariate orthonormalized B-splines.

3.5. Output statistics and other properties

The SCE approximation $y_{\mathbf{m},\Xi}(\mathbf{X})$ can be viewed as a surrogate of $y(\mathbf{X})$. Therefore, relevant probabilistic characteristics of $y(\mathbf{X})$, including its moments and PDF, if they exist, can be estimated from the statistical properties and probability law of this approximation.

Applying the expectation operator on $y_{\mathbf{m},\Xi}(\mathbf{X})$ in (23) and recognizing (21), the mean of the SCE approximation

$$\mu_{\mathbf{m},\Xi} := \mathbb{E}\left[y_{\mathbf{m},\Xi}(\mathbf{X})\right] = C_{\mathbf{1},\mathbf{m},\Xi} =: \mathbb{E}\left[y(\mathbf{X})\right] =: \mu, \ \mathbf{1} = (1, \ldots, 1), \tag{25}$$

is independent of $\mathbf{m}$ and Ξ and the same as the exact mean μ of the original function, provided that the expansion coefficient $C_{\mathbf{1},\mathbf{m},\Xi}$ is determined exactly.

Applying the expectation operator on $[y_{\mathbf{m},\Xi}(\mathbf{X}) - C_{\mathbf{1},\mathbf{m},\Xi}]^2$ and employing (21) and (22) results in the variance

$$\sigma^2_{\mathbf{m},\Xi} := \mathbb{E}\left[y_{\mathbf{m},\Xi}(\mathbf{X}) - \mu_{\mathbf{m},\Xi}\right]^2 = \sum_{\mathbf{i}\in I_{\mathbf{n}}} C^2_{\mathbf{i},\mathbf{m},\Xi} - C^2_{\mathbf{1},\mathbf{m},\Xi} \le \mathbb{E}\left[y(\mathbf{X}) - \mu\right]^2 =: \sigma^2 \tag{26}$$

of the SCE approximation, which is bounded by the exact variance σ^2 of the original function. Therefore, the second-moment properties of the SCE approximation are solely determined by the relevant expansion coefficients. The formulae of the second-moment properties for the SCE approximation are the same as those reported for the PCE approximation, although the respective expansion coefficients involved are not. The primary reason for this similarity is rooted in the use of the orthonormal basis in both expansions.

For high-order moments of $y(\mathbf{X})$ and its SCE approximation $y_{\mathbf{m},\Xi}(\mathbf{X})$, define their respective skewnesses

$$\gamma := \mathbb{E}\left[\left\{\frac{y(\mathbf{X}) - \mu}{\sigma}\right\}^3\right],\ \gamma_{\mathbf{m},\Xi} := \mathbb{E}\left[\left\{\frac{y_{\mathbf{m},\Xi}(\mathbf{X}) - \mu_{\mathbf{m},\Xi}}{\sigma_{\mathbf{m},\Xi}}\right\}^3\right], \tag{27}$$

and respective kurtoses

$$\kappa := \mathbb{E}\left[\left\{\frac{y(\mathbf{X}) - \mu}{\sigma}\right\}^4\right],\ \kappa_{\mathbf{m},\Xi} := \mathbb{E}\left[\left\{\frac{y_{\mathbf{m},\Xi}(\mathbf{X}) - \mu_{\mathbf{m},\Xi}}{\sigma_{\mathbf{m},\Xi}}\right\}^4\right]. \tag{28}$$

Unfortunately, no simple formulae from the SCE approximation, as obtained for the second-moment properties, can be derived for skewness and kurtosis. However, once the SCE approximation is constructed, any p-order moments can be calculated by analytical or numerical integration or resampling $y_{\mathbf{m},\Xi}(\mathbf{X})$ in conjunction with Monte Carlo or quasi Monte Carlo simulation or others.

In the following section, the convergence of SCE-generated p-order moments, including convergences in probability and in distribution, will be demonstrated. In this case, the PDF of $y(\mathbf{X})$, if it exists, can also be estimated economically by resampling $y_{\mathbf{m},\Xi}(\mathbf{X})$, to be illustrated in numerical examples.

3.6. Computational cost

The computational cost and complexity of SCE approximation with respect to stochastic dimension N can be judged by examining the corresponding numbers of basis functions involved. To do so, consider the SCE approximation in (23), where the total number of basis functions is

$$L_{\mathbf{m},\Xi} = \prod_{k=1}^{N} n_k. \tag{29}$$

Here, the number of basis functions n_k in the kth coordinate direction can be ascertained from the length of selected knot sequence $\boldsymbol{\xi}_k$ and degree of splines m_k. If $n_k = n$ for all $k = 1, \ldots, N$, then $L_{\mathbf{m},\Xi} = \mathcal{O}(n^N)$. Hence, given a fixed value of n, the computational effort with respect to N grows exponentially for the SCE approximation. Therefore, SCE like PCE also suffers from the curse of dimensionality. Having said this, SCE is still useful for fundamental studies on low-dimensional UQ problems, to be presented in Section 5.

4. L^p convergence of SCE

When using SCE or any other approximations it is important to provide estimates of the error measure. A convenient approach for such error analysis entails the modulus of smoothness of the function being approximated [17–19].

4.1. Modulus of smoothness

Loosely speaking, the modulus of smoothness describes the structural properties of the function and, prominently, its smoothness. In general, the smoother a function is, the faster it is approximated. Formal definitions of the modulus of smoothness in each coordinate direction k, followed by a tensorized version, are presented as follows.

Definition 2 (*Schumaker [18]*)**.** For the interval $[a_k, b_k]$ in the coordinate direction k, let $\alpha_k \in \mathbb{N}$ be a positive integer, $L^p(a_k, b_k)$, $2 \le p < \infty$, an unweighted normed space, and $0 < h_k \le (b_k - a_k)/\alpha_k$. Then the α_kth modulus of smoothness of a function $y(x_k) \in L^p[a_k, b_k]$ in the L^p-norm is a function defined by

$$\omega_{\alpha_k}(y; h_k)_{L^p[a_k,b_k]} := \sup_{0\le u_k\le h_k} \left\|\Delta^{\alpha_k}_{u_k} y(x_k)\right\|_{L^p[a_k, b_k - \alpha_k u_k]},\quad h_k > 0, \tag{30}$$

where

$$\Delta^{\alpha_k}_{u_k} y(x_k) := \sum_{i=0}^{\alpha_k} (-1)^{\alpha_k - i} \binom{\alpha_k}{i} y(x_k + i u_k)$$

is the α_kth forward difference of y at x_k for any $0 \le u_k \le h_k$.

Moreover, for a multi-index $\boldsymbol{\alpha} = (\alpha_1, \ldots, \alpha_N) \in \mathbb{N}^N$ and any vector $\mathbf{u} \ge \mathbf{0}$, let

$$\Delta^{\boldsymbol{\alpha}}_{\mathbf{u}} = \prod_{k=1}^{N} \Delta^{\alpha_k}_{u_k}.$$

Then, given the unweighted normed space $L^p\left(\mathbb{A}^N\right)$, the $\boldsymbol{\alpha}$-modulus of smoothness of a function $y(\mathbf{x}) \in L^p(\mathbb{A}^N)$ in the L^p-norm is the function defined by

$$\omega_{\boldsymbol{\alpha}}(y; \mathbf{h})_{L^p(\mathbb{A}^N)} := \sup_{\mathbf{0}\le\mathbf{u}\le\mathbf{h}} \left\|\Delta^{\boldsymbol{\alpha}}_{\mathbf{u}} y(\mathbf{x})\right\|_{L^p(\mathbb{A}^N_{\boldsymbol{\alpha},\mathbf{u}})},\quad \mathbf{h} > \mathbf{0}, \tag{31}$$

where

$$\mathbb{A}^N_{\boldsymbol{\alpha},\mathbf{u}} = \left\{\mathbf{x} \in \mathbb{A}^N : \mathbf{x} + \boldsymbol{\alpha} \otimes \mathbf{u} \in \mathbb{A}^N\right\},\quad \boldsymbol{\alpha} \otimes \mathbf{u} = (\alpha_1 u_1, \ldots, \alpha_N u_N).$$

4.2. Error analysis

A proposition and two lemmas are presented here to aid in development of a mathematical proof for the convergence of SCE.

Proposition 3. *For $y(\mathbf{x}) \in L^p(\mathbb{A}^N, \mathcal{B}^N, f_{\mathbf{X}}d\mathbf{x})$, $2 \le p < \infty$, and the spline space $\mathcal{S}_{\mathbf{m},\Xi}$ associated with degree $\mathbf{m}$ and family of knot sequences Ξ, the orthogonal projection operator $P_{\mathcal{S}_{\mathbf{m},\Xi}} : L^p(\mathbb{A}^N, \mathcal{B}^N, f_{\mathbf{X}}d\mathbf{x}) \to \mathcal{S}_{\mathbf{m},\Xi}$, defined by*

$$P_{\mathcal{S}_{\mathbf{m},\Xi}} y := \sum_{\mathbf{i}\in I_{\mathbf{n}}} C_{\mathbf{i},\mathbf{m},\Xi} \Psi_{\mathbf{i},\mathbf{m},\Xi}(\mathbf{x}), \tag{32}$$

is linear and bounded.

The proof is omitted here as it is similar to the one presented for an L^2 projection operator [12]. Interested readers should consult the prior work.

Lemma 4 (*Hölder's Inequality*)**.** *Let $s, t \in [1, \infty]$ such that $1/s + 1/t = 1$. Then for all measurable real-valued functions g, h on $\mathbb{A}^N$*

$$\|gh\|_{L^1(\mathbb{A}^N)} \le \|g\|_{L^s(\mathbb{A}^N)} \|h\|_{L^t(\mathbb{A}^N)}, \tag{33}$$

where $\|\cdot\|_{L^q(\mathbb{A}^N)}$ is an L^q-norm of the unweighted normed space $L^q\left(\mathbb{A}^N\right)$, $q \in [1, \infty]$.

Lemma 5. *Let*

$$L^p\left(\mathbb{A}^N\right) := \left\{y : \mathbb{A}^N \to \mathbb{R} : \int_{\mathbb{A}^N} |y(\mathbf{x})|^p d\mathbf{x} < \infty\right\},\ 2 \le p < \infty, \tag{34}$$

be an unweighted normed space of functions $y(\mathbf{x})$ with the standard norm

$$\|y(\mathbf{x})\|_{L^p(\mathbb{A}^N)} := \left(\int_{\mathbb{A}^N} y^2(\mathbf{x})\mathrm{d}\mathbf{x}\right)^{1/p}. \tag{35}$$

Then, for any function $y(\mathbf{x}) \in L^p(\mathbb{A}^N, \mathcal{B}^N, f_{\mathbf{X}}d\mathbf{x})$ and $f_{\mathbf{X}} \in L^\infty(\mathbb{A}^N)$, it holds that

$$\|y(\mathbf{x})\|_{L^p(\mathbb{A}^N,\mathcal{B}^N,f_{\mathbf{X}}d\mathbf{x})} \le \|y(\mathbf{x})\|_{L^p(\mathbb{A}^N)} \left(\left\|f_{\mathbf{X}}(\mathbf{x})\right\|_{L^\infty(\mathbb{A}^N)}\right)^{1/p}, \tag{36}$$

where $\|\cdot\|_{L^\infty(\mathbb{A}^N)}$ is the infinity norm.

Proof. From definition,

$$\begin{aligned} \|y(\mathbf{x})\|^p_{L^p(\mathbb{A}^N,\mathcal{B}^N,f_{\mathbf{X}}d\mathbf{x})} &:= \int_{\mathbb{A}^N} |y(\mathbf{x})|^p f_{\mathbf{X}}(\mathbf{x})d\mathbf{x} \\ &= \left\||y(\mathbf{x})|^p f_{\mathbf{X}}(\mathbf{x})\right\|_{L^1(\mathbb{A}^N)} \\ &\le \left\||y(\mathbf{x})|^p\right\|_{L^1(\mathbb{A}^N)} \cdot \left\|f_{\mathbf{X}}(\mathbf{x})\right\|_{L^\infty(\mathbb{A}^N)} \\ &= \|y(\mathbf{x})\|^p_{L^p(\mathbb{A}^N)} \cdot \left\|f_{\mathbf{X}}(\mathbf{x})\right\|_{L^\infty(\mathbb{A}^N)} \end{aligned} \tag{37}$$

where the third line stems from Hölder's inequality in Lemma 4 with the selection of $s = 1$ and $t = \infty$. As $\left\|f_{\mathbf{X}}(\mathbf{x})\right\|_{L^\infty(\mathbb{A}^N)}$ is positive, applying the pth-root on the last line of (37) yields the desired result. □

Theorem 6. *For any $y(\mathbf{X}) \in L^p(\Omega, \mathcal{F}, \mathbb{P})$, $2 \le p < \infty$, and a chosen degree $\mathbf{m}$ and family of knot sequences $\boldsymbol{\Xi}$, let $\{y_{\mathbf{m},\boldsymbol{\Xi}}(\mathbf{X})\}_{\mathbf{h}>\mathbf{0}}$, with $\mathbf{h} = (h_1, \ldots, h_N)$ representing the vector of largest element sizes, be a sequence of SCE approximations such that $y_{\mathbf{m},\boldsymbol{\Xi}}(\mathbf{X}) \in L^p(\Omega, \mathcal{F}, \mathbb{P})$. Then the sequence $\{y_{\mathbf{m},\boldsymbol{\Xi}}(\mathbf{X})\}_{\mathbf{h}>\mathbf{0}}$ converges to $y(\mathbf{X})$ in the pth mean or L^p sense, that is,*

$$\lim_{\mathbf{h}\to\mathbf{0}} \mathbb{E}\left[\left|y(\mathbf{X}) - y_{\mathbf{m},\boldsymbol{\Xi}}(\mathbf{X})\right|^p\right] = 0.$$

Proof. According to Proposition 3, $P_{S_{\mathbf{m},\boldsymbol{\Xi}}}$ is a linear, bounded operator. Therefore, with the tensor modulus of smoothness in mind, use Theorem 12.8 of Schumaker's book [18] to claim that the unweighted L^p-error from the SCE approximation is bounded by

$$\left\|y(\mathbf{x}) - y_{\mathbf{m},\boldsymbol{\Xi}}(\mathbf{x})\right\|_{L^p(\mathbb{A}^N)} \le C'\omega_{\mathbf{m}+\mathbf{1}}(y;\mathbf{h})_{L^p(\mathbb{A}^N)},\ 2 \le p < \infty, \tag{38}$$

where $\mathbf{m}+\mathbf{1} = (m_1+1, \ldots, m_N+1)$, $\omega_{\mathbf{m}+\mathbf{1}}(y;\mathbf{h})_{L^p(\mathbb{A}^N)}$ is the $(\mathbf{m}+\mathbf{1})$-modulus of smoothness of $y(\mathbf{x})$, and C' is a constant that depends only on $\mathbf{m}$, p, and N but not on the function y. Combining (37) from Lemma 5 and (38) produces

$$\left\|y(\mathbf{x}) - y_{\mathbf{m},\boldsymbol{\Xi}}(\mathbf{x})\right\|_{L^p(\mathbb{A}^N,\mathcal{B}^N,f_{\mathbf{X}}d\mathbf{x})} \le C\omega_{\mathbf{m}+\mathbf{1}}(y;\mathbf{h})_{L^p(\mathbb{A}^N)}, \tag{39}$$

as the weighted L^p-error from the SCE approximation, where

$$C := C'\left(\left\|f_{\mathbf{X}}(\mathbf{x})\right\|_{L^\infty(\mathbb{A}^N)}\right)^{1/p}$$

is another constant that depends on $\mathbf{m}$, p, N, and now also $f_{\mathbf{X}}$. However, it is still independent of the function y.

Eq. (39) describes an L^p distance of a function y to the spline space $S_{\mathbf{m},\boldsymbol{\Xi}}$ in terms of the modulus of smoothness of y. From Definition 2, as the element size h_k approaches *zero*, so does $0 \le u_k \le h_k$. Taking the limit $u_k \to 0$ inside the integral of the L^p norm, which is permissible for a finite interval and uniformly convergent integrand, the forward difference

$$\lim_{u_k\to 0} \Delta^{\alpha_k}_{u_k} y(x_k) = y(x_k) \sum_{i=0}^{\alpha_k} (-1)^{\alpha_k - i} \binom{\alpha_k}{i} = 0,$$

as the sum vanishes for any $\alpha_k \in \mathbb{N}$. Consequently, the coordinate modulus of smoothness

$$\omega_{\alpha_k}(y;h_k)_{L^p[a_k,b_k]} \to 0 \ \text{ as } h_k \to 0 \ \ \forall \alpha_k \in \mathbb{N}.$$

Following similar considerations, the tensor modulus of smoothness

$$\omega_{\boldsymbol{\alpha}}(y;\mathbf{h})_{L^p(\mathbb{A}^N)} \to 0 \ \text{ as } \mathbf{h} \to \mathbf{0} \ \ \forall \boldsymbol{\alpha} \in \mathbb{N}^N.$$

Therefore, the weighted L^p-error

$$\lim_{\mathbf{h}\to\mathbf{0}} \left\|y(\mathbf{x}) - y_{\mathbf{m},\boldsymbol{\Xi}}(\mathbf{x})\right\|_{L^p(\mathbb{A}^N,\mathcal{B}^N,f_{\mathbf{X}}d\mathbf{x})} = 0, \tag{40}$$

thus proving the L^p convergence of $y_{\mathbf{m},\boldsymbol{\Xi}}(\mathbf{X})$ to $y(\mathbf{X})$ for any degree $\mathbf{m} \in \mathbb{N}_0^N$ and $2 \le p < \infty$. Moreover, the smoother the function y is, the faster its modulus or the error vanishes and vice versa. □

4.3. A few remarks

From Theorem 6, the L^p convergence implies convergence in L^q, where $0 < q \le p$. Therefore, the SCE approximation converges in at most the pth mean. In other words, all moments of $y_{\mathbf{m},\boldsymbol{\Xi}}(\mathbf{X})$ of order up to and including p converge to the respective moments of $y(\mathbf{X})$, if they exist.

In addition, as the SCE approximation converges in the pth mean ($2 \le p < \infty$), it does so in probability. Moreover, as the expansion converges in probability, it also converges in distribution. This is because an L^p convergence, where $p \ge 2$, is stronger than the convergence in probability or in distribution.

5. Numerical examples

Four sets of numerical examples describing one-, two-, and four-dimensional output functions of input random variables are presented. While these functions are elementary, they are relevant, if not adequate, for conducting higher-order moment analysis. In all examples, the random input $\mathbf{X}$ fulfills Assumption 1, and the output function $y(\mathbf{X})$ is in $L^p(\Omega, \mathcal{F}, \mathbb{P})$, $p \ge 2$. Therefore, all second- and higher-order moments studied exist and are finite. The chief objective is to evaluate the power of the SCE approximation in computing various statistical moments and/or PDF of $y(\mathbf{X})$ and contrast the SCE results with those obtained from the existing PCE approximation.

The coordinate degrees for the SCE approximation in the third and fourth examples are identical, that is, $m_1 = m_2 = m_3 = m_4 = m$ (say). So are the knot sequences for SCE, that is, $\xi_1 = \xi_2 = \xi_3 = \xi_4 = \xi$ (say) with a uniform mesh of element sizes $h_1 = h_2 = h_3 = h_4 = h$. In all three examples, the spline degree m and/or the element size h were varied as appropriate. The basis functions for an mth-order PCE approximation are orthonormal Legendre (Examples 1, 3, and 4) or Hermite (Example 2) polynomials in input variables, whereas the basis functions for an SCE approximation, given a degree m and an element size h, are orthonormalized B-splines generated using the Cholesky factorization of the spline moment matrix. From the uniform or Gaussian distribution, the spline moment matrix was constructed analytically. All knot sequences are $(m+1)$-open and consist of uniformly spaced distinct knots with even and/or odd numbers of elements, depending on the example.

For a given function $y(\mathbf{X})$, denote by $y_{m,h}(\mathbf{X}) := y_{\mathbf{m},\boldsymbol{\Xi}}(\mathbf{X})$ an SCE approximation with degree $\mathbf{m}$, family of knot vectors $\boldsymbol{\Xi}$, and largest element size h, and by $y_m(\mathbf{X})$ an mth-order PCE approximation with the tensor-product truncation. The tensor-product truncation of PCE is consistent with the tensor-product truncation of SCE, ensuring a fair comparison between the two approximations. Let $\sigma^2_{m,h} := \sigma_{\mathbf{m},\boldsymbol{\Xi}}$, $\gamma_{m,h} := \gamma_{\mathbf{m},\boldsymbol{\Xi}}$, and $\kappa_{m,h} := \kappa_{\mathbf{m},\boldsymbol{\Xi}}$ be the variance, skewness, and kurtosis, respectively, of the SCE approximation and σ^2_m, γ_m, and κ_m the variance, skewness, and kurtosis, respectively, of the PCE approximation. Correspondingly, the respective relative errors committed by SCE in variance, skewness, and kurtosis are

$$e_{2,m,h} := \frac{\left|\sigma^2 - \sigma^2_{m,h}\right|}{\sigma^2},\ e_{3,m,h} := \frac{\left|\gamma - \gamma_{m,h}\right|}{\gamma},\ e_{4,m,h} := \frac{\left|\kappa - \kappa_{m,h}\right|}{\kappa} \tag{41}$$

and the respective relative errors perpetrated by PCE in the variance, skewness, and kurtosis are

$$e_{2,m} := \frac{\left|\sigma^2 - \sigma^2_m\right|}{\sigma^2},\ e_{3,m} := \frac{\left|\gamma - \gamma_m\right|}{\gamma},\ e_{4,m} := \frac{\left|\kappa - \kappa_m\right|}{\kappa}. \tag{42}$$

Here, σ^2, γ, and κ are the variance, skewness, and kurtosis of the output function $y(\mathbf{X})$, as defined in (26) through (28).

In all four examples, the variance, skewness, and kurtosis of the original function were determined by analytical integration and hence exactly. The SCE and PCE coefficients, which by definition are one- to four-dimensional integrals, were calculated analytically whenever possible or using adaptive numerical integration. While the second-moment properties of SCE/PCE were calculated using the formula in (25) and (26), the skewness and kurtosis of SCE/PCE approximations were calculated by either analytical or adaptive numerical integration. Therefore, all approximation errors reported in this paper were determined exactly or very accurately.

Although SCE provides a greater flexibility than PCE in exploiting low expansion orders, a comparison between the two approximations pertaining to their accuracy against computational effort is justified. The computational effort for such a comparison can be made by examining the total numbers of requisite basis functions from these approximations. As the numbers of univariate basis functions in all coordinate directions are identical – say, n for SCE and $m+1$ for PCE – the total number of basis functions from SCE and PCE approximations of an N-dimensional function are n^N and $(m+1)^N$, respectively.

5.1. Example 1: two univariate functions and bounded interval

Consider two univariate functions of a real-valued, uniformly distributed random variable X over the bounded interval $[-1, 1]$:

$$y(X) = \begin{cases} \dfrac{1}{1+5X^2}, & \text{(smooth)}, \\ \exp(-3|X|), & \text{(nonsmooth)}. \end{cases} \tag{43}$$

They comprise both smooth and non-differentiable (nonsmooth) functions, where the latter is more difficult to approximate by polynomials.

The analysis involved assessing (1) PCE approximations with nine increasingly large expansion orders m = 1, 2, 4, 8, 12, 16, 20, 24, 30 and (2) linear or first-order (m = 1) and quadratic or second-order (m = 2) SCE approximations, each endowed with six progressively refined mesh sizes of h = 1, 1/2, 1/4, 1/8, 1/12, 1/16. The knot sequences include uniformly spaced distinct knots and consist of even numbers of elements. For SCE, all internal knots are simple knots for the smooth function. However, for the nonsmooth function, all internal knots are either simple knots when m = 1 or include a repeated central knot when m = 2. The repeated central knot engenders aptly enriched basis functions, acquiring the nonsmooth behavior of the original function.

Figs. 2 and 3 display the comparisons of PCE and SCE approximations for the smooth and nonsmooth functions, respectively, of Example 1. For the smooth function [Fig. 2(a)], the maps of PCE approximations improve with m as expected. However, for the nonsmooth function [Fig. 3(a)], 20th- or higher-order PCE approximations are warranted for an acceptable map. In contrast, the maps of SCE approximations for the smooth function, exhibited in Fig. 2(b), look satisfactory, if not great, even for a linear spline (m = 1), as long as the mesh is adequately fine ($h \leq 1/4$). For the quadratic (m = 2) spline with $h \leq 1/4$, any distinction between the maps of an SCE approximation and actual function in Fig. 2(c) is indistinguishable to the naked eye. For the nonsmooth function, the maps of the original function and its quadratic SCE approximations in Fig. 3(c) for any mesh size are practically coincident.

All moments of orders of at least four obtained by SCE and PCE exist and are finite. Figs. 2(d) through 2(f) and Figs. 3(d) through 3(f) present the errors in variance ($e^2_{m,h}$, e^2_m), skewness ($e^3_{m,h}$, e^3_m), and kurtosis ($e^4_{m,h}$, e^4_m), obtained using SCE/PCE approximations of the smooth and nonsmooth functions, respectively. These errors are plotted against the requisite numbers of basis functions of SCE/PCE. When the function is globally smooth, as in Figs. 2(d) through 2(f), the errors caused by PCE are lower and decay faster than those committed by linear or quadratic SCE approximations for all three moments, especially when the number of basis functions is large. Therefore, existing PCE is adequate and there is no significant advantage of SCE over PCE approximations for smooth functions.

However, when calculating the three aforementioned moments of the nonsmooth function, as depicted in Figs. 3(d) through 3(f), there are notable differences in results from the SCE and PCE approximations. Clearly, the SCE approximation, regardless of its degree, commits much lower errors in variance, skewness, and kurtosis than does the PCE approximation for the same number of basis functions. Additionally, by placing a repeated central knot (multiplicity of two) in the knot sequence, the resulting quadratic SCE approximation has become substantially better than the linear SCE approximation. For all three moment calculations, the decay rate of error by either version of SCE is faster than that by PCE. Therefore, the SCE approximation proposed is desirable when there exist locally prominent and highly nonlinear stochastic responses, including discontinuity and nonsmoothness.

5.2. Example 2: two univariate functions and unbounded interval

Previously studied by Field and Grigoriu [20], the second example involves two univariate functions of a real-valued, standard Gaussian random variable X over the unbounded interval $(-\infty, \infty)$:

$$y(X) = \begin{cases} \Phi(X), & \text{(smooth)}, \\ |X|, & \text{(nonsmooth)}. \end{cases} \tag{44}$$

Here, $\Phi(u) = (1/\sqrt{2\pi}) \int_{-\infty}^{u} \exp(-\xi^2/2) d\xi$ is the cumulative probability distribution function of a Gaussian random variable with *zero* mean and *unit* variance. Again, both smooth and nonsmooth functions were selected. As opposed to Example 1, the unboundedness of random domain in Example 2 poses a challenge on the integrability of functions for higher-order moment analysis.

Here, the basis functions of PCE are orthonormal Hermite polynomials that are consistent with the standard Gaussian probability distribution of the input random variable. In contrast, the basis functions of SCE are orthonormal splines that are consistent with the truncated Gaussian probability distribution on the bounded interval $[-4, +4]$ of the input random variable. In addition, for SCE, the output function was transformed to a function of truncated Gaussian variable by matching the probability distribution functions of standard and truncated Gaussian variables. It is necessary to do so because splines require bounded support by definition. It is best practice to select a transformation yielding as little difference between the original and mapped distributions as is possible. Hence, the truncated Gaussian distribution is an appropriate choice for the transformation.

The analysis involves (1) PCE approximations for eight or nine distinct expansion orders of m = 1, 3, 5, 9, 13, 21, 29, 37 for the smooth function or m = 2, 4, 6, 8, 12, 16, 20, 24, 30 for the nonsmooth function and (2) linear (m = 1) and quadratic (m = 2) SCE approximations, each associated with eight distinct mesh sizes of h = 8/3, 8/5, 8/7, 8/9, 8/13, 8/17, 8/25, 8/33 for both functions. All internal knots are simple knots for both functions. By selecting odd numbers of elements, there are no central repeated knots for the nonsmooth function. If the number of elements were even, then SCE would reproduce the function exactly, creating an unfair comparison with PCE.

As before, Figs. 4 and 5 display the results of PCE and SCE approximations for the smooth and nonsmooth functions, respectively, from this example. The maps of both approximations improve with the order of PCE or the mesh refinement of the SCE, especially around the origin. However, as the distance from the origin increases, PCE yields greater oscillations than SCE. Still, the variance of the smooth function calculated by PCE, as presented in Fig. 4(d), is more accurate than that calculated by SCE for a fixed number of basis functions. The same behavior was observed for the smooth function in Example 1.This means that for a smooth function with bounded or unbounded random

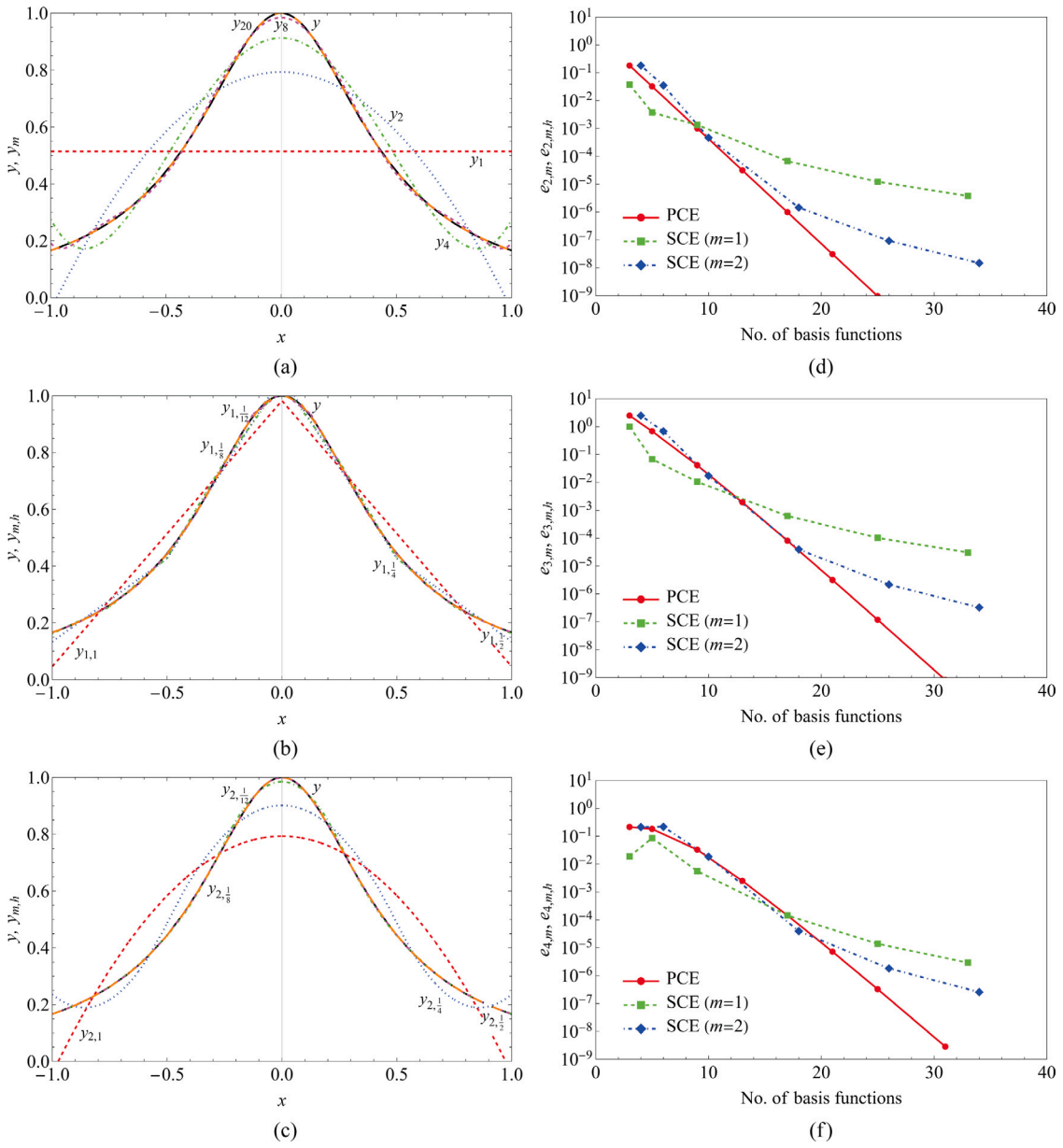

Fig. 2. Smooth function of Example 1: $y(X) = 1/(1+5X^2)$; (a) PCE approximations for m = 1, 2, 4, 8, 20; (b) linear ($m = 1$) SCE approximations for h = 1, 1/2, 1/4, 1/8, 1/12; (c) quadratic ($m = 1$) SCE approximations for h = 1, 1/2, 1/4, 1/8, 1/12; (d) relative errors in variance from SCE ($e_{2,m,h}$) and PCE ($e_{2,m}$); (e) relative errors in skewness from SCE ($e_{3,m,h}$) and PCE ($e_{3,m}$); (f) relative errors in kurtosis from SCE ($e_{4,m,h}$) and PCE ($e_{4,m}$).

domains, there is no need for SCE, as long as at most second-moment analysis is concerned. Conversely, when calculating higher-order moments, such as kurtosis in this example, PCE produces upward trending divergent solutions, as evidenced by Fig. 4(e). Here, as $x \to \pm\infty$, the oscillation from the fourth power of the PCE approximation escalates faster than the speed at which the Gaussian density function attenuates, consequently losing integrability when computing the fourth moment. This numerical result is consistent with the mathematical proof of divergence for the fourth moment of this function [21]. In contrast, the kurtosis estimated by SCE – be it linear or quadratic – in the same figure is convergent, as also proved theoretically in Section 4.

According to Figs. 5(a) and 5(b), the maps of SCE approximations for the nonsmooth function are stable even when extrapolated beyond $[-4, +4]$, whereas the maps of PCE approximations again exhibit considerable oscillations for large expansion orders. While these oscillations do not have yet deleterious effect on PCE's eventual convergence of variance [Fig. 5(d)], the decay rate slows down substantially. More importantly, the oscillations eventually become detrimental for higher-order moments of PCE, as alluded to earlier, leading to divergence when estimating skewness and kurtosis in Figs. 5(e) and 5(f). In fact, all PCE-generated moments of orders greater than four are divergent, as proved mathematically [21]. In contrast, the skewness and kurtosis evaluated by SCE approximations converge, albeit slowly owing to the nonsmoothness of the function. It would be interesting to study any improvement in the convergence properties of SCE for intervals larger than $[-4, +4]$ and non-uniform knot sequences.

5.3. Example 3: a nonsmooth bivariate function

Defined on the square $\mathbb{A}^2 = [-1, 1]^2$, consider a nonsmooth function of two uniformly distributed random variables X_1 and X_2, each distributed over $[-1, 1]$ [13]:

$$y(X_1, X_2) = g(X_1) + g(X_2) + \frac{1}{5} g(X_1) g(X_2), \tag{45}$$

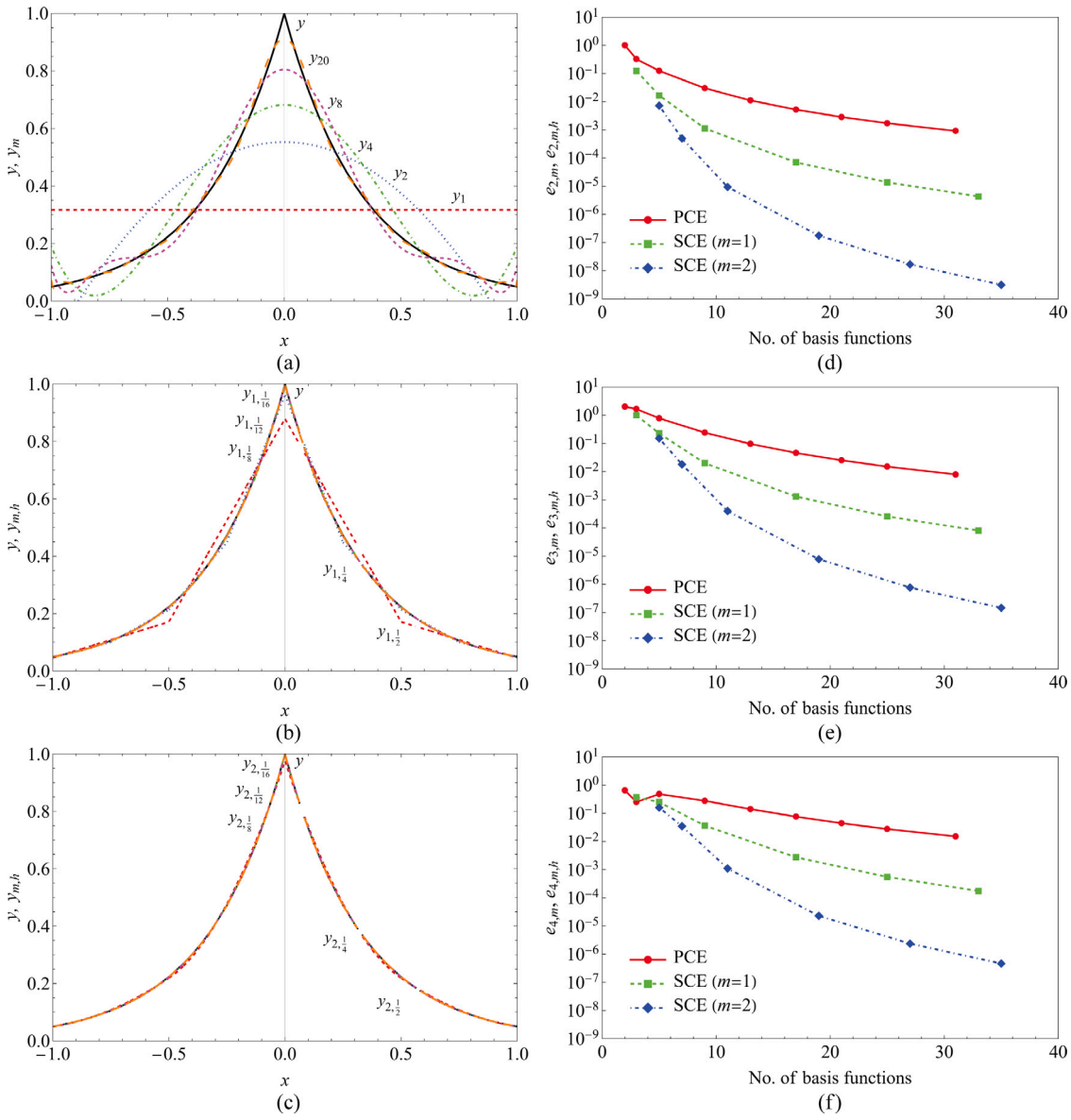

Fig. 3. Nonsmooth function of Example 1: $y(X) = \exp(-3|X|)$; (a) PCE approximations for m = 1, 2, 4, 8, 20; (b) linear ($m = 1$) SCE approximations for h = 1/2, 1/4, 1/8, 1/12, 1/16; (c) quadratic ($m = 2$) SCE approximations for h = 1/2, 1/4, 1/8, 1/12, 1/16; (d) relative errors in variance from SCE ($e_{2,m,h}$) and PCE ($e_{2,m}$); (e) relative errors in skewness from SCE ($e_{3,m,h}$) and PCE ($e_{3,m}$); (f) relative errors in kurtosis from SCE ($e_{4,m,h}$) and PCE ($e_{4,m}$).

where, for $i = 1, 2$,

$$g(x_i) = \begin{cases} 1, & -1 \le x_i \le 0, \\ \exp(-10x_i), & 0 < x_i \le 1. \end{cases} \tag{46}$$

A graph of the function in Fig. 6(a) indicates that y has a flat region on $[-1, 0]^2$, and then it falls off exponentially on both sides. Clearly, the function is continuous, but it has discontinuous partial derivatives across the lines $x_1 = 0$ and $x_2 = 0$. Figs. 6(b), 6(c), and 6(d) present graphs of a 20th-order PCE, a linear SCE with the mesh size of $h = 1/10$, and a quadratic SCE with the mesh size of $h = 1/10$, respectively. Given such a high order of expansion, the PCE approximation captures the overall trend well, but it is smoother than the original function. In contrast, the SCE approximations match the function very accurately, including replicating discontinuity of partial derivatives across the lines $x_1 = 0$ and $x_2 = 0$.

The analysis entails (1) PCE approximations for ten distinct values of $m = 1, 2, 4, 6, 8, 10, 12, 14, 16, 20$ and (2) linear ($m = 1$) and quadratic ($m = 2$) SCE approximations and ten distinct mesh sizes of $h = 2, 1, 1/2, 1/3, 1/4, 1/5, 1/6, 1/7, 1/8, 1/10$. The knot sequences include uniformly spaced distinct knots and consist of even numbers of elements. All internal knots are either simple knots when $m = 1$ or include a repeated central knot when $m = 2$.

Figs. 7(a) through 7(c) depict how the relative errors in variance, skewness, and kurtosis, calculated by various methods, decline against the number of basis functions. From these figures, the PCE approximation struggles to provide results as accurate as those obtained by the quadratic SCE approximation. This is largely due to the nonsmoothness in the original function y, as also observed in previous examples. Moreover, the convergence is steeper for quadratic SCE than linear SCE. However, the linear SCE becomes worse than PCE in calculating kurtosis when the number of basis functions is large. This is largely because of the uniform knots employed in such an SCE, mandating additional mesh refinements to reveal its true convergence properties. For instance, with the ad-hoc selection of a non-uniform knot sequence $\boldsymbol{\xi}_k = \{-1, -1, -0.5, 0, 0.01, 0.02, 0.03, 0.04, 0.05, 0.06, 0.08, 0.1, 0.15, 0.2, 0.25, 0.3, 0.35, 0.4, 0.45, 0.5, 0.75, 1, 1\}$, $k = 1, 2$, and requiring 441 basis functions, the linear SCE achieves the following errors: 1.94×10^{-6} for variance; 2.68×10^{-5} for skewness; and 1.25×10^{-6} for kurtosis. These errors are

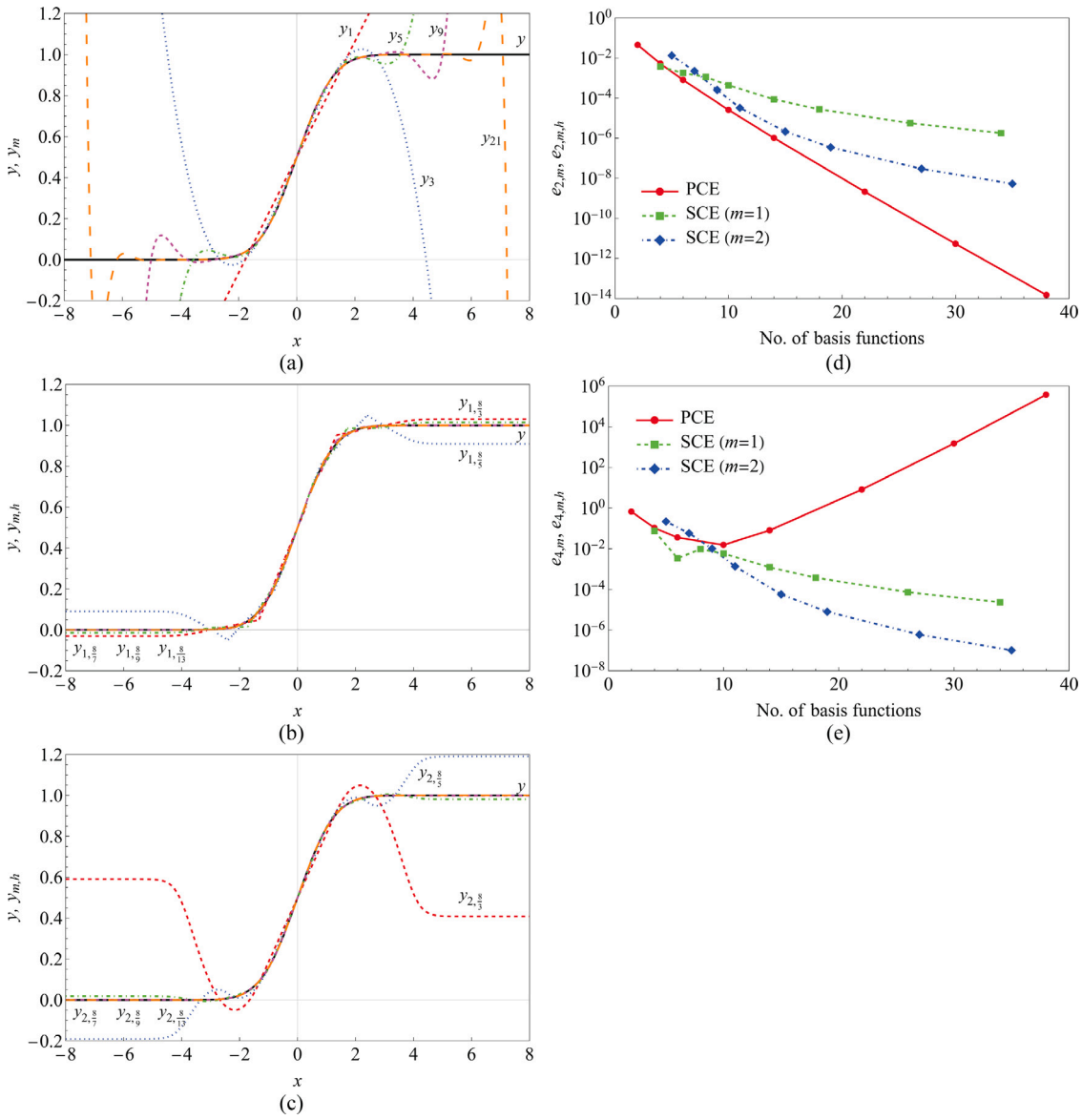

Fig. 4. Smooth function of Example 2: $y(X) = \Phi(X)$; (a) PCE approximations for $m = 1, 3, 5, 9, 21$; (b) linear ($m = 1$) SCE approximations for $h = 8/3, 8/5, 8/7, 8/9, 8/13$; (c) quadratic ($m = 1$) SCE approximations for $h = 8/3, 8/5, 8/7, 8/9, 8/13$; (d) relative errors in variance from SCE ($e_{2,m,h}$) and PCE ($e_{2,m}$); (e) relative errors in kurtosis from SCE ($e_{4,m,h}$) and PCE ($e_{4,m}$).

substantially lower than those committed by the 20th-order PCE or linear SCE with uniform knots ($h = 1/10$) in Figs. 7(a) through 7(c) (last points), each comprising 441 basis functions as well. In other words, an SCE with non-uniform knots is capable of producing more accurate statistics of the output variable than an SCE with uniform knots, depending on the function. The topic merits further study.

5.4. Example 4: a nonsmooth function of four variables

In the final example, a nonsmooth function

$$y(\mathbf{X}) = \prod_{i=1}^{4} \frac{|4X_i - 2|^{b_i} + a_i}{1 + a_i}, \quad a_i, b_i \in \mathbb{R}, \quad i = 1, 4, \tag{47}$$

of four independent random variables X_i, $i = 1, 2, 3, 4$, each of which is uniformly distributed over $[0, 1]$, was studied [12]. The function parameters are as follows: $a_1 = 0$, $a_2 = 1$, $a_3 = 2$, $a_4 = 4$; $b_1 = b_2 = b_3 = b_4 = 3/5$. Clearly, y is a non-differentiable function where the exponent b_i controls its nonlinearity. Compared with $b_i = 1$, the smaller the value of the exponent, the more nonlinear the function becomes in the ith coordinate direction. This type of function, especially with *unit* exponents, has been used for global sensitivity analysis [22].

Three approximation methods were used for UQ analysis in this example: (1) linear ($m = 1$) SCE approximations with two mesh sizes of $h = 1/2$ and $h = 1/8$; (2) quadratic ($m = 2$) SCE approximations with two mesh sizes of $h = 1/2$ and $h = 1/6$; and (3) 2nd- and 8th-order PCE approximations. Here, the two different mesh sizes of SCE and the two expansion orders of PCE represent their low-fidelity and high-fidelity approximations. In SCE calculations, there are even numbers of elements for the chosen meshes with repeated central knots ($x_k = 0.5$) in each coordinate direction. All distinct internal knots are uniformly spaced.

Table 1 lists the relative errors in calculating the variance, skewness, and kurtosis of $y(\mathbf{X})$ by the aforementioned three methods. The numbers of basis functions required for the low- and high-fidelity computations, defined by two respective variants of SCE and PCE approximations, are $3^4 = 81$ and $9^4 = 6561$, respectively. Therefore, the approximation quality of PCE and SCE can be assessed for the same computational effort. From Table 1, regardless of the fidelity of computations, the

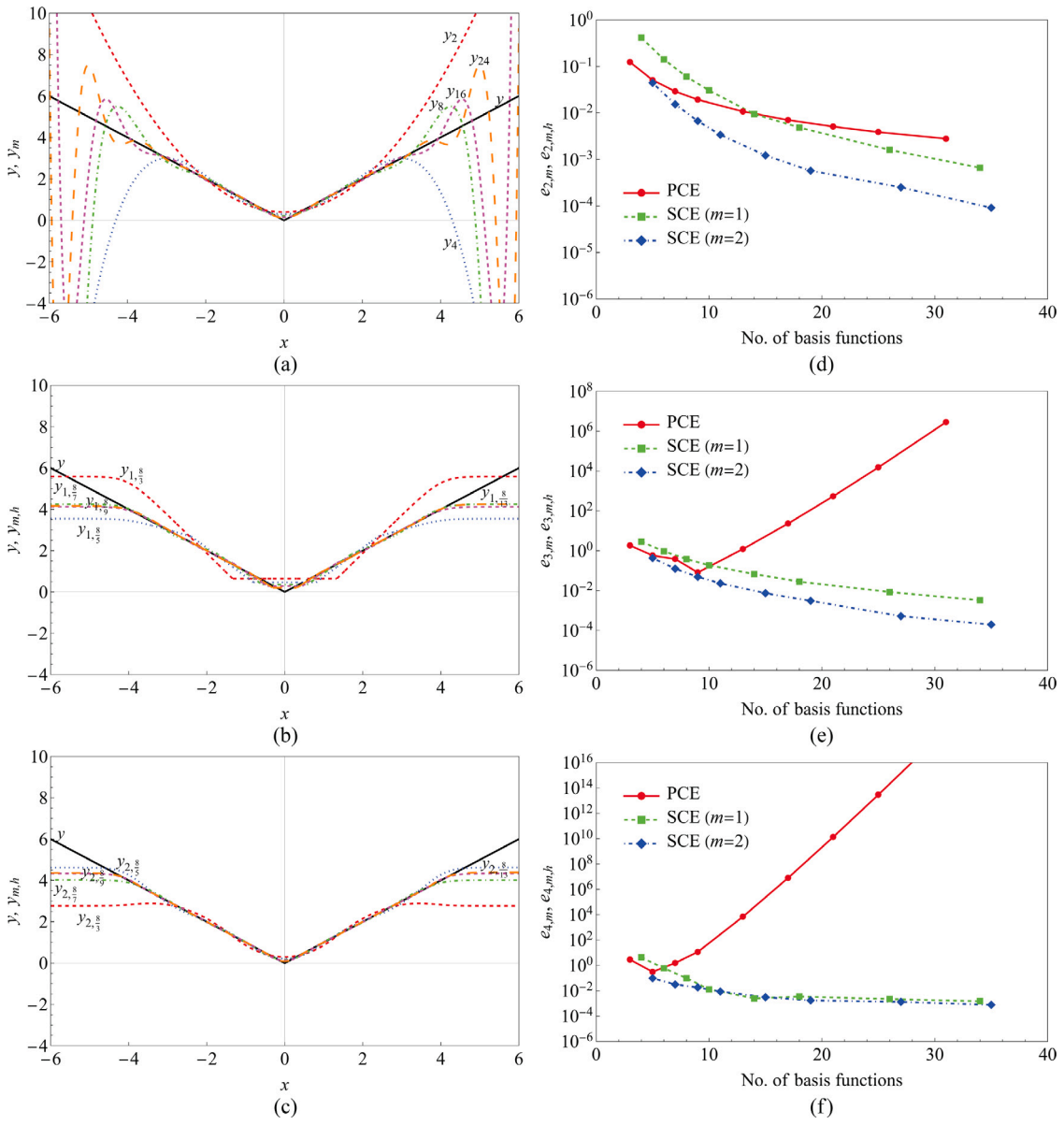

Fig. 5. Nonmooth function of Example 2: $y(X) = |X|$; (a) PCE approximations for m = 2, 4, 8, 16, 24; (b) linear (m = 1) SCE approximations for h = 8/3, 8/5, 8/7, 8/9, 8/13; (c) quadratic (m = 1) SCE approximations for h = 8/3, 8/5, 8/7, 8/9, 8/13; (d) relative errors in variance from SCE ($e_{2,m,h}$) and PCE ($e_{2,m}$); (e) relative errors in skewness from SCE ($e_{3,m,h}$) and PCE ($e_{3,m}$); (f) relative errors in kurtosis from SCE ($e_{4,m,h}$) and PCE ($e_{4,m}$).

errors in all three moments committed by SCE (linear or quadratic) are orders of magnitudes lower than those perpetrated by PCE. This is mainly due to the non-differentiability of $y(\mathbf{X})$.

Since there does not exist analytical means to determine the probabilistic characteristics of $y(\mathbf{X})$ and its surrogates, the PCE and SCE approximations once built were re-sampled to generate their associated PDFs. In addition, crude MCS of the original function was also performed to obtain a reference PDF. The sample sizes for crude MCS and re-sampling are 100,000. The PDFs obtained from the PCE and SCE approximations and crude MCS are depicted in Fig. 8. The results indicate that low-order SCE approximations [Figs. 8(b) or 8(c)] with a sufficiently refined mesh also yield more accurate estimates of PDF than a high-order PCE approximation [Fig. 8(a)] for nonsmooth functions.

6. Discussion

While the paper is aimed at calculating higher-order moments of SCE, its application is limited to solving low-dimensional UQ problems

Table 1
Relative errors in calculating the variance, skewness, and kurtosis of the nonsmooth function in Example 4 by various PCE and SCE approximations.

(a) mth-order PCE				
m	No. of basis	$e_{2,m}$	$e_{3,m}$	$e_{4,m}$
2	81	0.15741175	3.166336594	0.60883659
8	6561	0.01751586	0.35450758	0.03748577
(b) Linear SCE (m = 1)				
h	No. of basis	$e_{2,1,h}$	$e_{3,1,h}$	$e_{4,1,h}$
1/2	81	0.02478277	1.3184678	0.14332562
1/8	6561	0.00140325	0.04716611	0.01266868
(c) Quadratic SCE (m = 2)				
h	No. of basis	$e_{2,2,h}$	$e_{3,2,h}$	$e_{4,2,h}$
1/2	81	0.00375152	0.15045514	0.04509998
1/6	6561	0.00055234	0.01699404	0.00612819

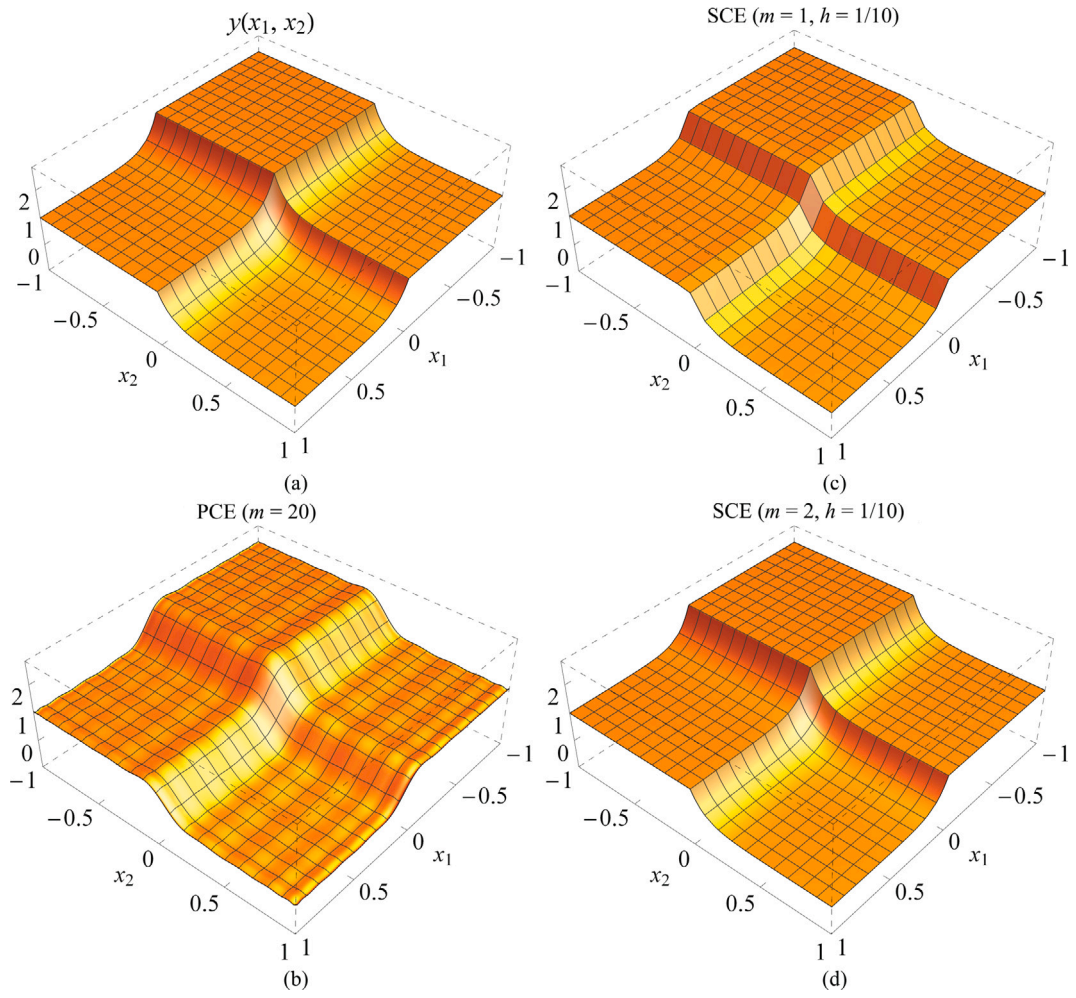

Fig. 6. Graphs of functions in Example 3: (a) exact; (b) 20th-order PCE (c) linear SCE with $h = 1/10$; (d) quadratic SCE with $h = 1/10$;.

($N \leq 10$). This is essentially because of the tensor-product structure in forming the multivariate basis of SCE. For high-dimensional problems ($N \geq 10$), SCE becomes computationally prohibitive, raising the need for SDD, as briefly mentioned in the Introduction section. However, as SDD is built on dimensionwise decomposition and involves only low-dimensional tensor products of univariate basis functions, the convergence properties of SCE should extend to SDD as well. Therefore, the theoretical and numerical results of SCE presented here are relevant for a general UQ analysis.

The refinements of SCE in the Example section are predicated on knot sequences with uniform spacing in all coordinate directions. As a result, the resulting basis is not necessarily maximally empowered to capture locally abrupt changes in stochastic responses, if they exist, in an efficient manner. Therefore, future endeavors employing optimally selected non-uniform knot sequences, as studied by the author's group in the context of SDD [23], should be undertaken for calculating higher-order moments of SCE more effectively.

For the quadratic SCE approximations in some examples, repeated central knots have been used to recognize the lack of differentiability in the output function. In doing so, the resulting basis functions of SCE become equipped to capture accurately the nonsmooth behavior of the original function. In practice, such manipulations of the knot sequences are not possible in general if the presence or locations of nonsmoothness are not known *a priori*. Therefore, an adaptive scheme for automatically detecting possible nonsmoothness and their locations should be developed in conjunction with the SCE approximation.

It is well established over the last few decades that PCE works well for a wide range of UQ problems in engineering and applied sciences. This is chiefly because the underlying performance functions are globally smooth, explaining why PCE's globally supported polynomials are well-suited to approximate such functions, resulting in accurate and efficient estimates of second-moment statistics. However, for multi-scale or multi-component complex systems involving multiple failure modes, one may face nonsmooth or even discontinuous functions in which the behavior of PCE has not been studied extensively. Therefore, future works on higher-order moment analysis by SCE and PCE for large-scale, practical problems featuring smooth and nonsmooth functions are warranted.

7. Conclusion

A UQ analysis entailing high-order moments calculated from SCE approximations of a real-valued, p-integrable ($2 \leq p < \infty$) output function of input random variable was conducted. The approximation quality of SCE was assessed in terms of the modulus of smoothness of the function. When the largest element of the mesh from SCE approaches zero, the modulus of smoothness vanishes, resulting in the L^p convergence of SCE to the correct limit. Therefore, the moment of SCE of an order up to and including p converges to the exact moment for any degree of splines as the element size decreases. Moreover, the weaker modes of convergence, such as those in probability and in distribution, transpire naturally.

Numerical computations of moments by SCE and PCE, conducted for a collection of simple yet relevant examples, indicate the following:

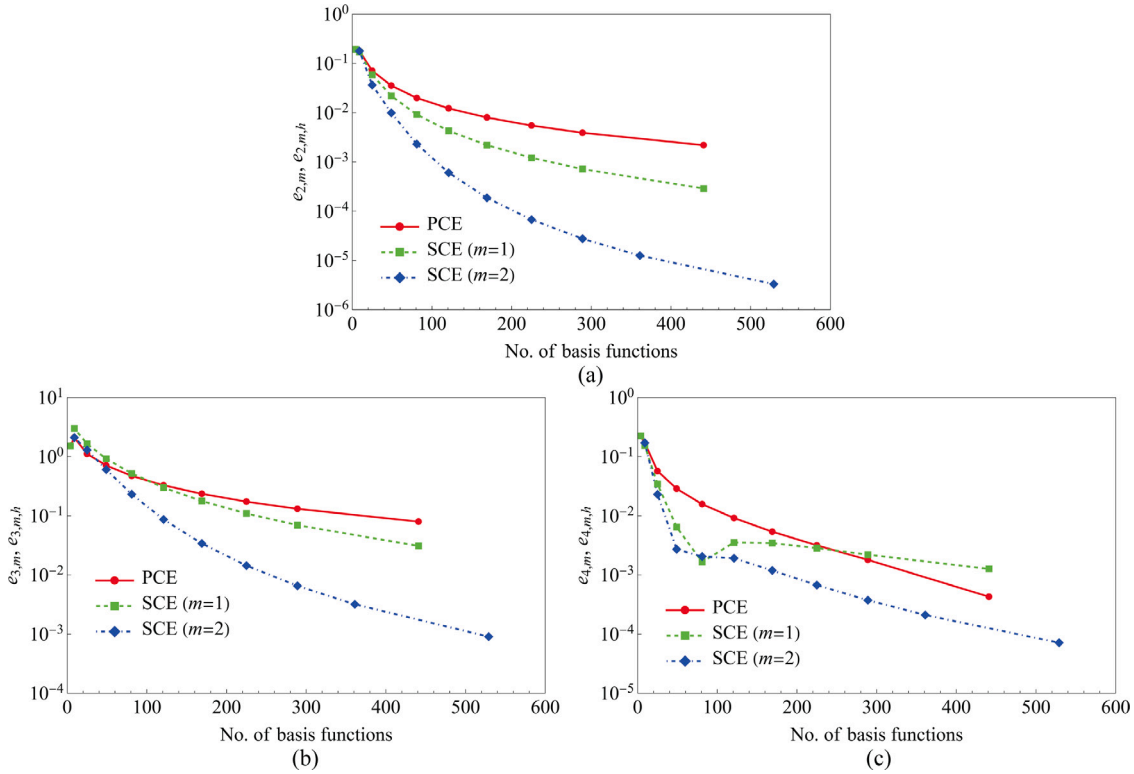

Fig. 7. Relative errors from various SCE and PCE approximations of the nonmooth function in Example 3: (a) variance ($e_{2,m,h}$, $e_{2,m}$); (b) skewness ($e_{3,m,h}$, $e_{3,m}$); (c) kurtosis ($e_{4,m,h}$, $e_{4,m}$).

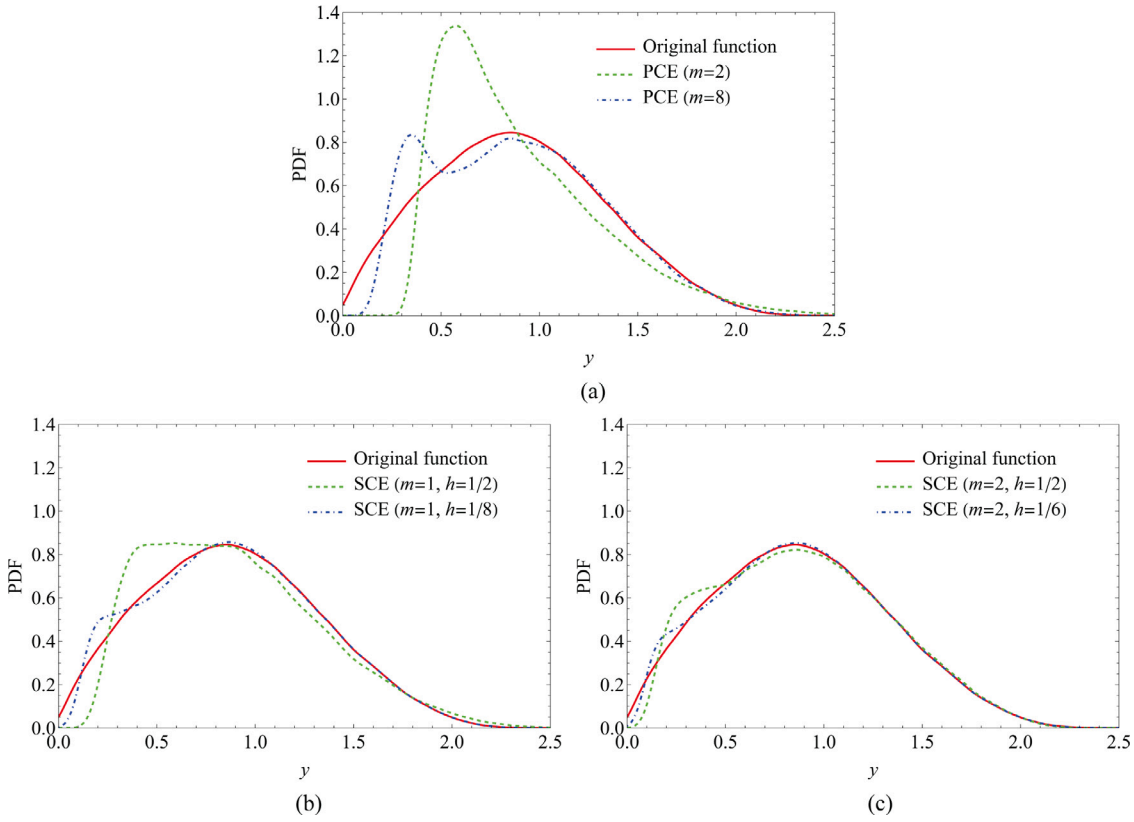

Fig. 8. Probability density functions of $y(\mathbf{X})$ estimated by three methods: (a) PCE; (b) linear SCE; (c) quadratic SCE.

(1) When the output function is smooth or nonsmooth and the random domain is bounded or unbounded, SCE and PCE both provide convergent estimates of the variance. However, their relative convergent rates may differ, depending on the smoothness of the function.
(2) When the function is globally smooth, PCE is likely to provide more efficient estimates of variance than SCE for the same computational effort. However, for a nonsmooth function, the trend reverses, and the convergence properties of PCE in estimating variance may degrade appreciably.
(3) Higher-order moments, such as skewness and kurtosis, calculated using SCE converge for all examples considered in this study. In contrast, moments of PCE of orders larger than two may or may not converge, depending on the regularity of the output function or the probability measure of input random variables.

CRediT authorship contribution statement

Sharif Rahman: Writing – review & editing, Writing – original draft, Visualization, Validation, Supervision, Software, Resources, Project administration, Methodology, Investigation, Funding acquisition, Formal analysis, Data curation, Conceptualization.

Declaration of competing interest

The authors declare that they have no known competing financial interests or personal relationships that could have appeared to influence the work reported in this paper.

Data availability

Data will be made available on request.

Appendix. Univariate B-splines

Let $\mathbf{x} = (x_1, \ldots, x_N)$ be an arbitrary point in $\mathbb{A}^N$. For the coordinate direction k, $k = 1, \ldots, N$, define a positive integer $n_k \in \mathbb{N}$ and a non-negative integer $m_k \in \mathbb{N}_0$, representing the total number of basis functions and polynomial degree, respectively. The rest of this appendix briefly describes paraphernalia of univariate B-splines.

A.1. Knot vector

In order to define B-splines, the concept of knot vector, also referred to as knot sequence, for each coordinate direction k is needed.

Definition 7. A knot vector $\boldsymbol{\xi}_k$ for the interval $[a_k, b_k] \subset \mathbb{R}$, given $n_k > m_k \geq 0$, is a vector comprising a non-decreasing sequence of real numbers

$$\begin{aligned}\boldsymbol{\xi}_k := \{\xi_{k,i_k}\}_{i_k=1}^{n_k+m_k+1} = \{a_k = \xi_{k,1}, \xi_{k,2}, \ldots, \xi_{k,n_k+m_k+1} = b_k\},\\ \xi_{k,1} \leq \xi_{k,2} \leq \cdots \leq \xi_{k,n_k+m_k+1},\end{aligned} \tag{A.1}$$

where ξ_{k,i_k} is the i_kth knot with $i_k = 1, 2, \ldots, n_k + m_k + 1$ representing the knot index for the coordinate direction k. The elements of $\boldsymbol{\xi}_k$ are called knots.

According to (A.1), there are a total of $n_k + m_k + 1$ knots, which may be equally or unequally spaced. To monitor knots without repetitions, denote by $\zeta_{k,1}, \ldots, \zeta_{k,r_k}$ the r_k distinct knots in $\boldsymbol{\xi}_k$ with respective multiplicities $M_{k,1}, \ldots, M_{k,r_k}$. Then the knot vector in (A.1) can be expressed more compactly by

$$\begin{aligned}\boldsymbol{\xi}_k = \{a_k = \overbrace{\zeta_{k,1}, \ldots, \zeta_{k,1}}^{M_{k,1} \text{ times}}, \overbrace{\zeta_{k,2}, \ldots, \zeta_{k,2}}^{M_{k,2} \text{ times}}, \ldots,\\ \overbrace{\zeta_{k,r_k-1}, \ldots, \zeta_{k,r_k-1}}^{M_{k,r_k-1} \text{ times}}, \overbrace{\zeta_{k,r_k}, \ldots, \zeta_{k,r_k}}^{M_{k,r_k} \text{ times}} = b_k\},\\ a_k = \zeta_{k,1} < \zeta_{k,2} < \cdots < \zeta_{k,r_k-1} < \zeta_{k,r_k} = b_k,\end{aligned} \tag{A.2}$$

which consists of a total number of

$$\sum_{j_k=1}^{r_k} M_{k,j_k} = n_k + m_k + 1 \tag{A.3}$$

knots. As shown in (A.2), each knot, whether interior or exterior, may appear $1 \leq M_{k,j_k} \leq m_k + 1$ times, where M_{k,j_k} is referred to as its multiplicity. The multiplicity has important implications on the regularity properties of B-spline functions. A knot vector is called open if the end knots have multiplicities $m_k + 1$. In this case, definitions of more specific knot vectors are in order.

Definition 8. A knot vector is said to be $(m_k + 1)$-open if the first and last knots appear $m_k + 1$ times, that is, if

$$\begin{aligned}\boldsymbol{\xi}_k = \{a_k = \overbrace{\zeta_{k,1}, \ldots, \zeta_{k,1}}^{m_k+1 \text{ times}}, \overbrace{\zeta_{k,2}, \ldots, \zeta_{k,2}}^{M_{k,2} \text{ times}}, \ldots,\\ \overbrace{\zeta_{k,r_k-1}, \ldots, \zeta_{k,r_k-1}}^{M_{k,r_k-1} \text{ times}}, \overbrace{\zeta_{k,r_k}, \ldots, \zeta_{k,r_k}}^{m_k+1 \text{ times}} = b_k\},\\ a_k = \zeta_{k,1} < \zeta_{k,2} < \cdots < \zeta_{k,r_k-1} < \zeta_{k,r_k} = b_k.\end{aligned} \tag{A.4}$$

Definition 9. A knot vector is said to be $(m_k + 1)$-open with simple knots if it is $(m_k + 1)$-open and all interior knots appear only once, that is, if

$$\begin{aligned}\boldsymbol{\xi}_k = \{a_k = \overbrace{\zeta_{k,1}, \ldots, \zeta_{k,1}}^{m_k+1 \text{ times}}, \zeta_{k,2}, \ldots, \zeta_{k,r_k-1}, \overbrace{\zeta_{k,r_k}, \ldots, \zeta_{k,r_k}}^{m_k+1 \text{ times}} = b_k\},\\ a_k = \zeta_{k,1} < \zeta_{k,2} < \cdots < \zeta_{k,r_k-1} < \zeta_{k,r_k} = b_k.\end{aligned} \tag{A.5}$$

A $(m_k + 1)$-open knot vector with or without simple knots is commonly found in applications [15].

A.2. B-splines

The B-spline functions for a given degree are defined in a recursive manner using the knot vector as follows.

Definition 10. Let $\boldsymbol{\xi}_k$ be a general knot vector of length at least $m_k + 2$ for the interval $[a_k, b_k]$, as defined by (A.1). Denote by $B^k_{i_k,m_k,\boldsymbol{\xi}_k}(x_k)$ the i_kth univariate B-spline function with degree $m_k \in \mathbb{N}_0$ for the coordinate direction k. Given the *zero*-degree basis functions,

$$B^k_{i_k,0,\boldsymbol{\xi}_k}(x_k) := \begin{cases} 1, & \xi_{k,i_k} \leq x_k < \xi_{k,i_k+1}, \\ 0, & \text{otherwise}, \end{cases} \tag{A.6}$$

for $k = 1, \ldots, N$, all higher-order B-spline functions on $\mathbb{R}$ are defined recursively by

$$\begin{aligned}B^k_{i_k,m_k,\boldsymbol{\xi}_k}(x_k) = \frac{x_k - \xi_{k,i_k}}{\xi_{k,i_k+m_k} - \xi_{k,i_k}} B^k_{i_k,m_k-1,\boldsymbol{\xi}_k}(x_k)\\ + \frac{\xi_{k,i_k+m_k+1} - x_k}{\xi_{k,i_k+m_k+1} - \xi_{k,i_k+1}} B^k_{i_k+1,m_k-1,\boldsymbol{\xi}_k}(x_k),\end{aligned} \tag{A.7}$$

where $1 \leq k \leq N$, $1 \leq i_k \leq n_k$, $1 \leq m_k < \infty$, and $0/0$ is considered as zero.

The recursive formula in Definition 10 was derived by Cox [24] and de Boor [16].

References

[1] M. Grigoriu, Stochastic Calculus: Applications in Science and Engineering, Birkhauser, 2002.
[2] T.J. Sullivan, Introduction to Uncertainty Quantification, New York, Springer, 2015.
[3] N. Wiener, The homogeneous chaos, Amer. J. Math. 60 (4) (1938) 897–936.

[4] R.H. Cameron, W.T. Martin, The orthogonal development of non-linear functionals in series of Fourier-Hermite functionals, Ann. of Math. 48 (1947) 385–392.
[5] R. Ghanem, P.D. Spanos, Stochastic finite elements: a spectral approach, World Publishing Corp., 1991.
[6] S. Rahman, A polynomial dimensional decomposition for stochastic computing, Internat. J. Numer. Methods Engrg. 76 (2008) 2091–2116.
[7] S. Rahman, Mathematical properties of polynomial dimensional decomposition, SIAM/ASA J. Uncertain. Quantif. 6 (2018) 816–844.
[8] I. Babuska, F. Nobile, R. Tempone, A stochastic collocation method for elliptic partial differential equations with random input data, SIAM J. Numer. Anal. 45 (3) (2007) 1005–1034.
[9] D. Xiu, J.S. Hesthaven, High-order collocation methods for the differential equation with random inputs, SIAM J. Sci. Comput. 27 (2005) 1118–1139.
[10] S. Smolyak, Quadrature and interpolation formulas for tensor products of certain classes of functions, Dokl. Akad. Nauk SSSR 4 (1963) 240–243.
[11] T. Gerstner, M. Griebel, Numerical integration using sparse grids, Numer. Algorithms 18 (1998) 209–232.
[12] S. Rahman, A spline chaos expansion, SIAM/ASA J. Uncertain. Quantif. 8 (2020) 27–57.
[13] S. Rahman, R. Jahanbin, A spline dimensional decomposition for uncertainty quantification in high dimensions, SIAM/ASA J. Uncertain. Quantif. 27 (2005) 1118–1139.
[14] C. Eckert, M. Beer, P. Spanos, A polynomial chaos method for arbitrary random inputs using B-splines, Probab. Eng. Mech. 60 (2020) 1–9.
[15] J.A. Cottrell, T.J.R. Hughes, Y. Bazilevs, Isogeometric Analysis: Toward Integration of CAD and FEA, John Wiley & Sons, 2009.
[16] C. De Boor, On calculation with B-splines, J. Approx. Theory 6 (1972) 50–62.
[17] W. Dahmen, R. de Vore, K. Scherer, Multi-dimensional spline approximation, SIAM J. Numer. Anal. 17 (1980) 380–402.
[18] L.J. Schumaker, Spline Functions: Basic Theory, third ed., Cambridge, Cambridge University Press, 2007.
[19] A.F. Timan, Theory of Approximation of Functions of a Real Variable, New York, Dover Publication, 1994.
[20] R.V. Field, M.D. Grigoriu, On the accuracy of the polynomial chaos approximation, Probab. Eng. Mech. 191 (2004) 65–80.
[21] R. Field, M. Grigoriu, Convergence Properties of Polynomial Chaos Approximations for L_2 Random Variables, Tech. Rep., (SAND2007-1262) Sandia National Laboratory, 2007.
[22] A. Saltelli, I.M. Sobol, About the use of rank transformation in sensitivity analysis of model output, Reliab. Eng. Syst. Saf. 50 (1995) 225–239.
[23] S. Dixler, R. Jahanbin, S. Rahman, Uncertainty quantification by optimal spline dimensional decomposition, Internat. J. Numer. Methods Engrg. 122 (2021) 5898–5934.
[24] M.G. Cox, The numerical evaluation of B-splines, J. Inst. Math. Appl. 10 (1972) 134–149.